Correlations between Cortical and Locomotor Muscle in the Seven Gait Phases during Treadmill Walking

Pengna Wei
Xi'an Jiaotong University
Jinhua Zhang (jjshua@mail.xjtu.edu.cn)
Xi'an Jiaotong University https://orcid.org/0000-0002-1178-2058
Baozeng Wang
Xi'an Jiaotong University
Jun Hong
Xi'an Jiaotong University

Research

Keywords: Electroencephalo gram (EEG), Surface electromyography (sEMG), Gait 50 phases, Time frequency cross mutual information (TFCMI)

Posted Date: February 6th, 2020

DOI: https://doi.org/10.21203/rs.2.22753/v1

Correlations between Cortical and Locomotor Muscle in the Seven Gait Phases during Treadmill Walking

Pengna Wei[1], Jinhua Zhang[1*], Baozeng Wang[1], Jun Hong[1]
[1]The Key Laboratory of Education Ministry for Modern Design and Rotor-Bearing System, School of Mechanical Engineering, Xi'an Jiaotong University, Xi'an, China

Corresponding author: Jinhua Zhang

Pengna Wei is with the Key Laboratory of Education Ministry for Modern Design and Rotor-Bearing System, School of Mechanical Engineering, Xi'an Jiaotong University, Xi'an, China (e-mail: penny0218@stu.xjtu.edu.cn)

Jinhua Zhang is with the Key Laboratory of Education Ministry for Modern Design and Rotor-Bearing System, School of Mechanical Engineering, Xi'an Jiaotong University, Xi'an, China (e-mail: jjshua@mail.xjtu.edu.cn.).

Baozeng Wang is with the Key Laboratory of Education Ministry for Modern Design and Rotor-Bearing System, School of Mechanical Engineering, Xi'an Jiaotong University, Xi'an, China (e-mail: baoer723166@163.com)

Jun Hong is with the Key Laboratory of Education Ministry for Modern Design and Rotor-Bearing System, School of Mechanical Engineering, Xi'an Jiaotong University, Xi'an, China (e-mail: jhong@mail.xjtu.edu.cn)

Abstract

Background: Previous researchers have found that cortex is involved in the regulation of treadmill walking. However, cortico-muscular interaction analysis in a 'fine' gait phase (such as seven phases of the gait cycle) remains lacking in the time-frequency domain.

Methods: In this investigation, we used beta band electroencephalogram (EEG) data to find that eight muscle-related cortices are inconsistent at the end of the swing and stance phases. The eight muscle-related cortices differ at each phase according to gamma band EEG data. Firstly, slope sign change (SSC) and mean power frequency (MPF) features of EEG and surface electromyography (sEMG) were used to recognize the seven gait phases, which are loading response (LR), mid-stance (MST), terminal stance (TST), pre-swing (PSW), initial swing (ISW), mid-swing (MSW) and terminal swing (TSW). Following this, the time-frequency cross mutual information (TFCMI) method, a novel time-frequency analysis method, was applied to examine the eight muscle-related cortices in seven gait phases using beta and gamma band EEG data.

Results: We firstly found that the feature set comprising SSC of EEG as well as SSC and MPF of sEMG was available for seven gait phases recognition, and secondly that TFCMI values between each sEMG channel and EEG differed significantly in the seven gait phases.

Conclusions: This suggests that analysis of the seven gait phases is

beneficial. These insights enrich previous findings from authors carrying out cortico-muscular interaction analysis as well as providing critical information for rehabilitation physicians.

Keywords

Electroencephalogram (EEG); Surface electromyography (sEMG); Gait phases; Time-frequency cross mutual information (TFCMI)

Introduction

Human locomotor disorder seriously affects quality of life. Nontraumatic gait disorder is caused by brain damage and occurs in many neurological disorders such as stroke, cerebral palsy and Parkinson's disease[1][2][3]. Human bipedal walking is a complex activity which requires collaboration between the cerebral cortex, spinal cord and locomotor muscles. Several research groups have observed significant cortical activation (for example, in the premotor, supplementary motor and primary sensorimotor regions) during walking[4][5][6][7][8]. Additionally, the lower limb related cortical area precisely controls lower limb muscles during walking[9][4][10].

In 2018, Peter and colleagues found a significant increase in the central common drive through tibialis anterior - tibialis anterior and soleus - medial gastrocnemius EMG-EMG (electromyography) coherence analysis in beta and gamma frequencies during visually guided walking compared

with typical walking[11]. The next year, the same group found that the motor cortex contributes to both ankle plantar flexor muscle activity and forward propulsion during gait[12]. However, cortico-muscular connectivity remains unclear.

It is therefore crucial that the mechanisms of gait control in the cerebral cortex are understood. Authors of recent studies have found that gait phase is associated with cortical activity modulations[13][14][5][15]. Various researchers have used either coherence or correlation analysis methods to measure cortico-muscular coherence[12][4]. However, coherence and correlation analysis are suitable for linear signals, while both electroencephalogram (EEG) and surface electromyography (sEMG) signals are non-linear[16]. The time-frequency cross mutual information (TFCMI) method can be utilized to calculate mutual information between two time-frequency domain signals[17][18][19]. We used TFCMI to estimate the interaction between EEG and sEMG channels.

Every moment of the gait cycle activates the flexibility of several muscles to meet the needs of the environment. It is, therefore, necessary to explore the cortico-muscular connection of each gait phase. Despite this, most research groups have focused on the cortical activation of the two or four gait phases which can be detected by four footswitches attached to shoe soles[4]. Additionally, cortical activation in the fine gait phase has received little research attention. Therefore, we set out to investigate gait phase

recognition methods.

The human gait cycle is divided into stance and swing phases[20][21][22][23]. The stance phase is then sub-divided into loading response (LR), mid-stance (MST), terminal stance (TST) and pre-swing (PSW). Similarly, the swing phase is divided into initial swing (ISW), mid-swing (MSW) and terminal swing (TSW). More information about gait partitioning methods is available elsewhere in the literature[20]. However, recognition methods for the seven gait phases have received little research information due to the uniqueness of each individual's gait[24]. Additionally, gait phase recognition methods are incomplete, meaning they cannot identify all seven gait phases. For instance, Li and colleagues utilized EMG signals to recognize five gait phases[24], while Wei et al. applied sEMG and kinematic data from both legs to recognize five gait phases[25].

In this study, we used sEMG, EEG signals and 3D motion trajectory data for lower limbs to identify all seven gait phases. EEG and sEMG signals, generated before movement, are the bioelectrical signals of the human body[2][26][27]. We have previously used these signals to identify the movement intentions of the human body and have applied them to rehabilitation devices[28][29]. In this study, we calculated TFCMI values between EEG and sEMG channels in the seven gait phases, using both beta and gamma band EEG data, following previous research[30][31].

Materials and methods

Participants and ethical approval

Nine healthy participants (seven males and two females, aged 23 to 26) were recruited from Xi'an Jiaotong University. All had medical certificates. All study procedures performed were approved by the Institutional Review Boards of Xi'an Jiaotong University and carried out according to the Helsinki Declaration of 1975.

Experimental device

The custom-designed equipment used in this experiment included: a treadmill, an electrode cap, an amplifier with a built-in 3-axis acceleration sensor, an sEMG electrode, a motion capture camera and a Vicon reflector ball, as shown in Figure 1 (a). We utilized a 32ch LiveAmp Cap with multitrodes to record EEG and sEMG signals during treadmill walking. This LiveAmp Cap was a customized, wireless, lightweight, wearable device, meaning it caused minimum disturbance to participants' movement while EEG and sEMG were recorded. The technical specifications of this device enable outstanding signal quality. A gaze screen with a cross symbol was used to focus participants, as shown in Figure 1 (b). Figure 1 (c) shows the lower limb model in a motion capture system. All participants walked on the treadmill using their typical walking style. Participants choose a

comfortable treadmill speed of 2.0 km/h during the experiment. The speeds of 1.4 km/h and 2.6 km/h were also selected to simulate slow and fast walking speeds in everyday life.

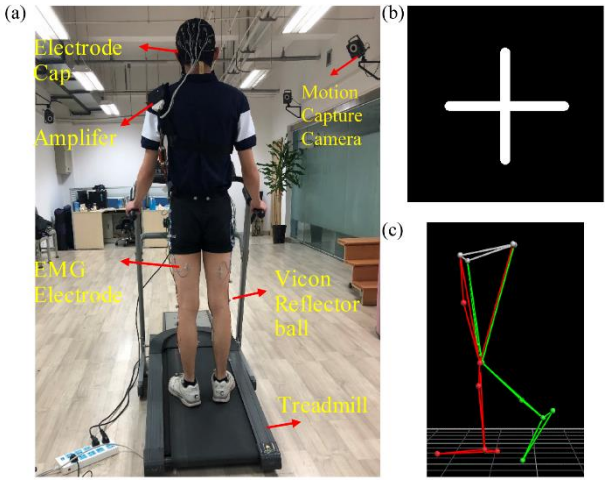

Fig. 1 (a) Experimental device, (b) cross symbol, (c) lower limb model in motion capture system.

Data collection

All participants walked on a treadmill at three speeds (1.4 km/h, 2.0 km/h and 2.6 km/h) respectively in 15 30-second time blocks. There was a break between any two training speeds. The initial 1-minute length of walking on the treadmill was adapted according to the experimental conditions. Participants were asked to walk as usual, as well as to relax and minimize eye blinks, head rotation and swallowing during the study. Participants were also asked to fix their gaze to the cross symbol, as shown in Figure 1 (b). Experiments were conducted in a quiet room and participants were asked to move as lightly as possible to reduce noise.

EEG, sEMG signals and lower limb trajectory data were simultaneously recorded. Some 24-channel EEG signals and eight muscles of the lower limb sEMG signals – that is, biceps femoris (BF), vastus medialis (VM), tibialis anterior (TA) and gastrocnemius medialis (GM), bilaterally – were collected by the 32Ch LiveAmp Cap with multitrodes at a sampling rate of 500Hz; 24 unipolar channels were collected in the cap and electrodes for eight bipolar sEMG were recorded at the legs. BF, VM, TA and GM were selected as they are related to the entire gait cycle[32][33]. Locations for sEMG electrodes were selected based on the SENIAM guidelines (www.seniam.org), while EEG electrodes were placed in accordance with the international 10-20 electrode system. Impedance of EEG and sEMG electrodes were kept under 20 kΩ throughout the experiment.

Signals were amplified using a wireless LiveAmp amplifier (Brain Products Inc., Gilching, Germany). The 16 positions (anterior superior iliac, posterior superior iliac, thigh, knee, tibia, ankle, heel and toe, bilaterally) of the lower limbs were acquired by 16 reflective markers, using a 10-camera motion capture system Nexus 2.6 (VICON T40S, UK) at a sampling rate of 100Hz. Reflective markers' positions are presented in Figure 1 (c). The motion capture system was synchronized with the wireless LiveAmp amplifier via the LiveAmp sensor and trigger extension. 3-D marker data were resampled and aligned to EEG and sEMG data using a Matlab (Mathworks Natick, MA, USA) script, based on the EEGLAB

toolbox[34] before further preprocessing.

Data processing

EEG and sEMG data processing

Raw EEG data were pre-processed using Brain Vision Analyzer 2.1 (Brain Products Inc., Gilching, Germany) and a Matlab (Mathworks Natick, MA, USA) script based on the EEGLAB toolbox, thus minimizing motion and other artifacts[35]. The raw signal processing flow can be seen in Figure 2. The default reference position of the electrode cap is FCz. However, FCz is too close to other EEG electrodes. Therefore, raw data were re-referenced to the mastoid, and the mean of the left and right mastoid signal was calculated as a new reference. The EEG, EOG and 3-axis acceleration channels of the amplifier were selected. EEG signals were then high-pass filtered using a zero-phase 0.5 Hz low cutoff and second-order Butterworth filter before being low-pass filtered using a zero-phase 50 Hz high cutoff and second-order Butterworth filter to remove high- and low-frequency noise, respectively. A zero-phase 50 Hz, second-order Butterworth filter was used to remove power frequency from the raw EEG signals.

The EEG data were resampled to 1000 Hz and independent component analysis (ICA)[36] was used to decompose EEG signals so they were maximally independent. The ICs which most correlated to lateral and vertical eye movement were marked and removed. sEMG signals were

passed through an elliptic bandpass filter of 50-450 Hz bandwidth while an FIR least-square bandstop notch filter of 50 Hz was used to acquire useful information from raw sEMG signals. Wavelet denoising technology with 'wden' and 'db4' basis functions was used to eliminate noise in sEMG signals. EEG and sEMG channels with obvious artifacts were removed following visual inspection.

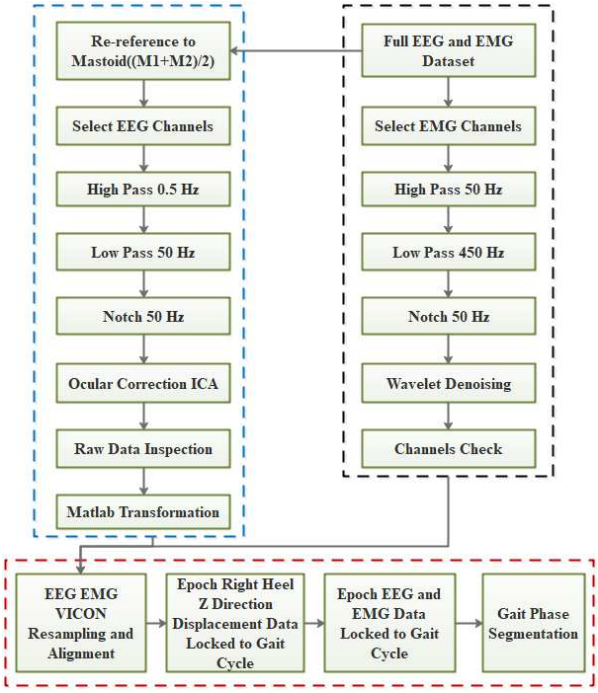

Fig. 2 Outline of data processing steps.

Gait cycle segmentation

3-D marker data from the 16 positions were used to divide the gait cycle during treadmill walking. Displacement in z direction of the right heel with a more obvious periodicity of the gait cycle than in other marker data was applied to divide EEG and sEMG signals into a single gait cycle. Results can be seen in Figure 3.

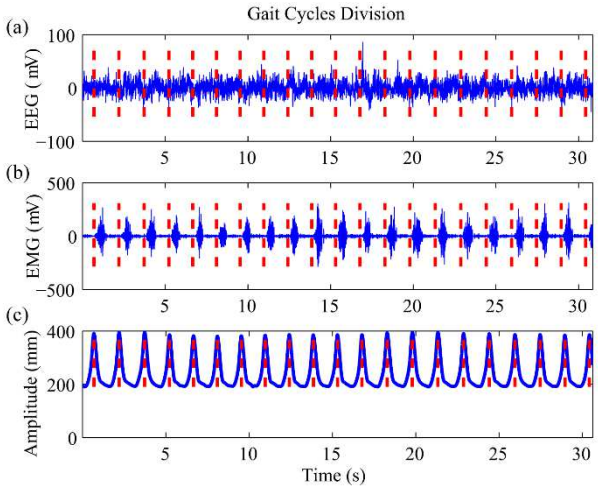

Fig. 3 (a) EEG signals, (b) sEMG signals, (c) displacement in z direction of right heel.

Gait phase segmentation

The seven gait phases are demarcated according to 3-D marker data from the 16 positions. The gait phase segmentation result can be seen in Figure 4. In Figure 4 (b), the first vertical red line – the first intersection of the z-direction trajectory data of right heel (Rheez) and the z-direction trajectory data of right toe (Rtoez) – indicates the endpoint of the middle swing. The second vertical red line – the point with the largest difference between the y-direction trajectory data of right heel (Rheey) plus the y-direction trajectory data of left heel (Lheey) – indicates the endpoint of the terminal swing. The third vertical red line – the first intersection of the Rheez and the z-direction trajectory data of left heel (Lheez) – indicates the endpoint of the loading response. The fourth vertical red line – the maximum point of the Lheez – indicates the endpoint of the middle stance. The fifth vertical

red line – the second intersection of the Rheez and the Rtoez – indicates the endpoint of the terminal stance. Finally, the sixth vertical red line – the point with the smallest difference between the Rheey and the Lheey – indicates the endpoint of the pre-swing.

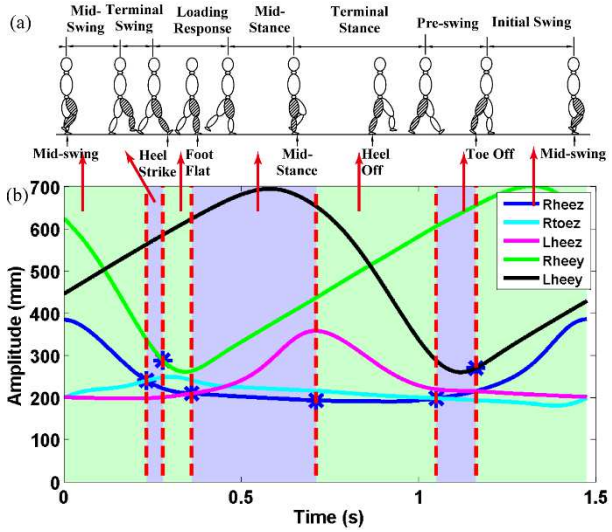

Fig. 4 Gait phase division results. (a) Seven gait phases of the gait cycle, (b) trajectory data.

Feature extraction

Feature extraction is a technique used to draw representation information from pre-processed input data. For analysis of sEMG and EEG signals, feature extraction methods tend to include time domain (TD), frequency domain (FD) and time-frequency (TFD) domain[37][38][39]. In this study, slope sign change (SSC) and mean power frequency (MPF) were utilized to classify the seven gait phases. SSC is a time domain feature which also reflects signal frequency information. It is defined as follows:

$$SSC = \sum_{j=2}^{m-1}[G[(y_j - y_{j-1}) \times (y_j - y_{j+1})]];$$
$$G(x) = \begin{cases} 1, & if \quad y \geq threshold \\ 0, & otherwise \end{cases} \tag{1}$$

where y_j is the signals at time point j and m is the length of the signals. MPF is a mean frequency which is expressed as the sum of sEMG and EEG power frequency, divided by the total sum of the spectrum intensity:

$$MPF = \frac{\int_1^N f \cdot S(f) df}{\int_1^N S(f) df} \tag{2}$$

where f is frequency of the spectrum and N is the length of the frequency bin. These extract features were inputted into LIBSVM for classification. LIBSVM parameters were optimized using the particle swarm optimization (PSO) method.

Time-frequency analysis using TFCMI

TFCMI values were calculated to estimate the time-frequency correlation between EEG and sEMG channels. EEG and sEMG signals were normalized due to their large power difference before calculating TFCMI. The calculation process can be seen below.

Morlet wavelet transformation, which contains both time and frequency domain information, was utilized to transform the EEG signal into the time-frequency domain[40]. Time-frequency power maps of each channel for beta (16-25 Hz) and gamma (30-45 Hz) data were created. Therefore, the two maps were 10×2000 and 16×2000 respectively. Ten and 16

represent the frequency from 16 to 25 Hz and 30 to 45 Hz while 2000 represents the sample points. The mean of beta and gamma band powers were calculated respectively before two 1×2000 power curves were created in each channel. The Morlet wavelet transformation can be calculated as:

$$W(a,b) = \int_{-x}^{x} x(t) \frac{1}{\sqrt{a}} \psi\left(\frac{t-b}{a}\right) dt,$$
$$\psi(x) = e^{-x^2} \cos\left(\pi \sqrt{\frac{2}{\ln 2}} x\right)$$

where a is scaling factor, b is translation factor, $\psi(x)$ is a mother (or Morlet) wavelet of wavelet transform.

Cross mutual information (CMI) between any two channels was calculated using the mean power signals. CMI maps were created by computing the entropy and mutual information, which can be expressed as:

$$H(F_i) = -\sum_{b=1}^{40} p(F_{i,b}) \log_2 p(F_{i,b})$$

$$TFMI(F_i, F_j) = H(F_i) + H(F_j) - H(F_i, F_j)$$
$$= \sum_{b=1}^{40} p(F_{i,b}, F_{j,b}) \log_2 \frac{p(F_{i,b}, F_{j,b})}{p(F_{i,b}) p(F_{j,b})}$$

where $H(F_i)$ denotes entropy, F_i is mean power signals at the ith channel, $p(F_{i,b})$ is the probability density function (PDF) of F_i, $p(F_{i,b}, F_{j,b})$ is the joint probability density function (JPDF) of F_i while F_j, $b = 1, 2, \cdots, 40$ is the bin number of the histogram used to construct the approximated PDF. Some 40 bins were selected based on both previous research and our data[41][42].

Finally, TFCMI values between any two channels were obtained to create

a 31×31 (23 EEG and eight sEMG channels) TFCMI map (Fig. 5 (a)). Each entry of the 31×31 matrix is the value of mutual information from TF power between a pair of channels. TFCMI values from the ith to the jth as well as the jth to the ith are the same. Therefore, the TFCMI map is symmetrical. Since TFCMI values were normalized, the diagonal TFCMI value (self-relevance) is equal to one. TFCMI values from the 13 EEG (lower limb movement-related electrodes: F3, F4, C3, C4, P3, P4, F7, F8, P7, P8, Fz, Cz, Pz) and eight sEMG channels were extracted from the 31×31 matrix. We then calculated the mean of TFCMI values between 13 EEG and eight sEMG channels in all trials, which were illustrated as a 13 channel topographic map. The map of mean coupling strength from Oz channel to all EEG channels as well as Fpz channel to all EEG channels can be seen in Figure 5 (b).

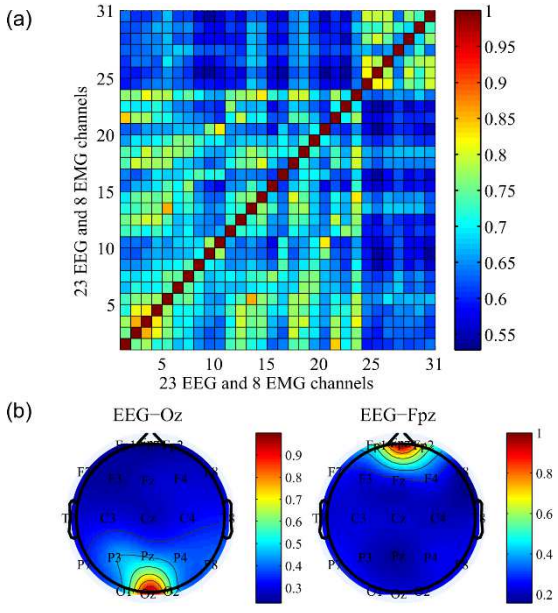

Fig. 5 TFCMI computation. (a) TFCMI map, (b) topographic map of mean coupling strength from Oz channel to all EEG channels and Fpz channel to

all EEG channels.

Results

Gait phase recognition results

It should be noted that the sEMG data of three participants are unavailable due to surface electrode malfunction. Therefore, this analysis is based on seven participants. Gait phase recognition was based on the SSC and MPF features of the sEMG and EEG signals. Firstly, we compared gait phase recognition based on the SSC and MPF features of sEMG with the SSC and MPF features of sEMG as well as the SSC feature of EEG. Secondly, gait phase recognition using the SSC and MPF features of sEMG and the SSC feature of EEG was compared with recognition using the SSC and MPF features of sEMG and the MPF feature of EEG.

Difference between sEMG and EEG signal features

Gait phase identification based on the feature set comprising SSC and MPF features of sEMG and identification based on the feature set comprising SSC and MPF features of sEMG as well as SSC feature of EEG are shown in Figure 6. Gait phase identification in the seven gait phases and three speeds (1.4 km/h, 2.0 km/h and 2.6 km/h) can be seen in Figures 6 (a), (b) and (c) respectively. Figure 6 (a) demonstrates that the mean accuracy of recognition of the seven gait phases using the two feature sets (SSC and

MPF of sEMG vs SSC and MPF of sEMG as well as SSC of EEG) were 93.47% and 95.58%. There was a slight increase when the SSC of EEG was applied, when the standard deviation (SD) decreased from 0.062 to 0.045. The same can be observed in Figures 6 (b) and (c). In Figure 6 (b), the mean accuracy of identifying the seven gait phases increased from 96.69% to 97.63%, while the SD decreased from 0.032 to 0.025. In Figure 6 (c), the mean accuracy of identifying the seven gait phases increased from 97.62% to 98.10%, while the SD decreased from 0.048 to 0.044.

A paired samples test was used to analyze whether the difference in gait phase recognition between the two feature sets was significant. We found that the difference between the two feature sets was significant at 1.4 km/h (p=0.017), but not at at 2.0 km/h (p=0.085) or 2.6 km/h (p=0.279). Results for each participant based on the SSC and MPF features of sEMG, as well as the SSC and MPF of sEMG and SSC of EEG, can be seen in supplementary material, Figures S1, S2 and S3.

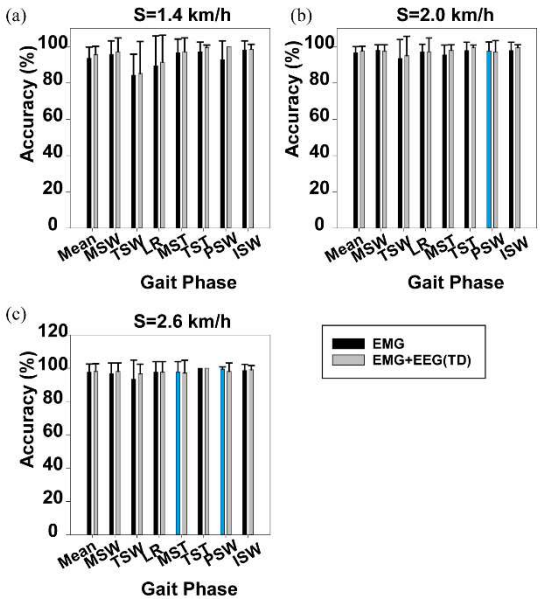

Fig. 6 Gait phase recognition results based on the SSC and MPF features of sEMG as well as results based on the SSC and MPF features of sEMG and SSC feature of EEG. (a) Walking speed 1.4 km/h, (b) walking speed 2.0 km/h, (c) walking speed 2.6 km/h. The blue column indicates that results based on sEMG features are better than sEMG features combined with the EEG feature of SSC.

Difference between the EEG features of the SSC and MPF

Figure 7 displays gait phase recognition based on the SSC and MPF of sEMG and the SSC of EEG as well as gait phase recognition based on the SSC and MPF of sEMG and the MPF of EEG. Gait phase recognition in seven phases at three speeds (1.4 km/h, 2.0 km/h and 2.6 km/h) can be seen in Figures 7 (a), (b) and (c) respectively. These figures demonstrate that the mean accuracy of recognition of the seven gait phases decreased from 95.58% to 71.90%, 97.63% to 80.63% and 98.10% to 87.89% respectively

while the SD increased from 0.045 to 0.158, 0.025 to 0.23 and 0.044 to 0.121, respectively when the SSC of EEG was replaced by the MPF of EEG. Some gait phase recognition results based on the SSC and MPF of sEMG and the MPF of EEG were below 60%, for example, PSW in Figures 7 (a), (b) and (c). Using statistical analysis, we found that the gait phase recognition difference between the two sets was significant at 1.4 km/h (p=0.000), 2.0 km/h (p=0.003) and 2.6 km/h (p=0.023).

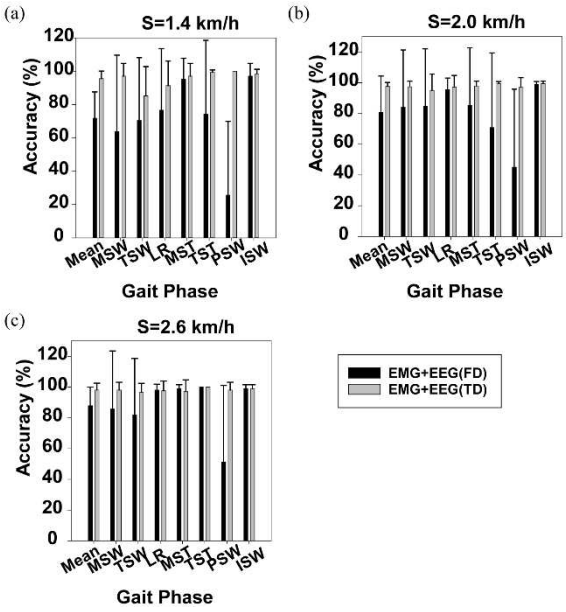

Fig. 7 Gait phase recognition based on the SSC and MPF of sEMG and the SSC of EEG as well as gait phase recognition based on the SSC and MPF of sEMG and the MPF of EEG. (a) Walking speed 1.4 km/h, (b) walking speed 2.0 km/h, (c) walking speed 2.6 km/h.

Time-frequency analysis of EEG and sEMG signals using TFCMI

We carried out a time-frequency analysis of the EEG and sEMG signals using TFCMI at a comfortable speed (2.0 km/h). TFCMI topography between EEG data (beta band) and sEMG of both the stance (LR, MST, TST, PSW) and swing phases (ISW, MSW, TSW) can be seen in Figures 8, 9, 10 and 11. Results in Figures 8 and 9 are based on the sEMG channels of right (Rt.) and left (Lt.) TA as well as right and left VM. Results in Figures 10 and 11 are based on the sEMG channels of BF and GM of both legs. In Figures 8 and 9, we can observe that the distribution of TFCMI values between EEG and TA differs from those between EEG and VM in PSW and TSW. Table 1 shows the sEMG channels most related to the EEG channels in PSW and TSW. TFCMI topography for gamma band is shown in the supplementary material; Figures S4, S5, S6 and S7.

Table 1 sEMG channels most related to EEG channels in PSW and TSW

Gait phases	sEMG channels	Most related EEG channels
PSW	Rt.TA	F4, Fz, P3
	Lt.TA	F4, Fz
	Rt.VM	F4, Fz, F3, C4 and Pz
	Lt.VM	F4, F3, P4

TSW	Rt.TA	F4, Fz, F3
	Lt.TA	C3, C4
	Rt.VM	F3, C4, F4
	Lt.VM	F4, F3, Fz, C4, Cz, P3, Pz

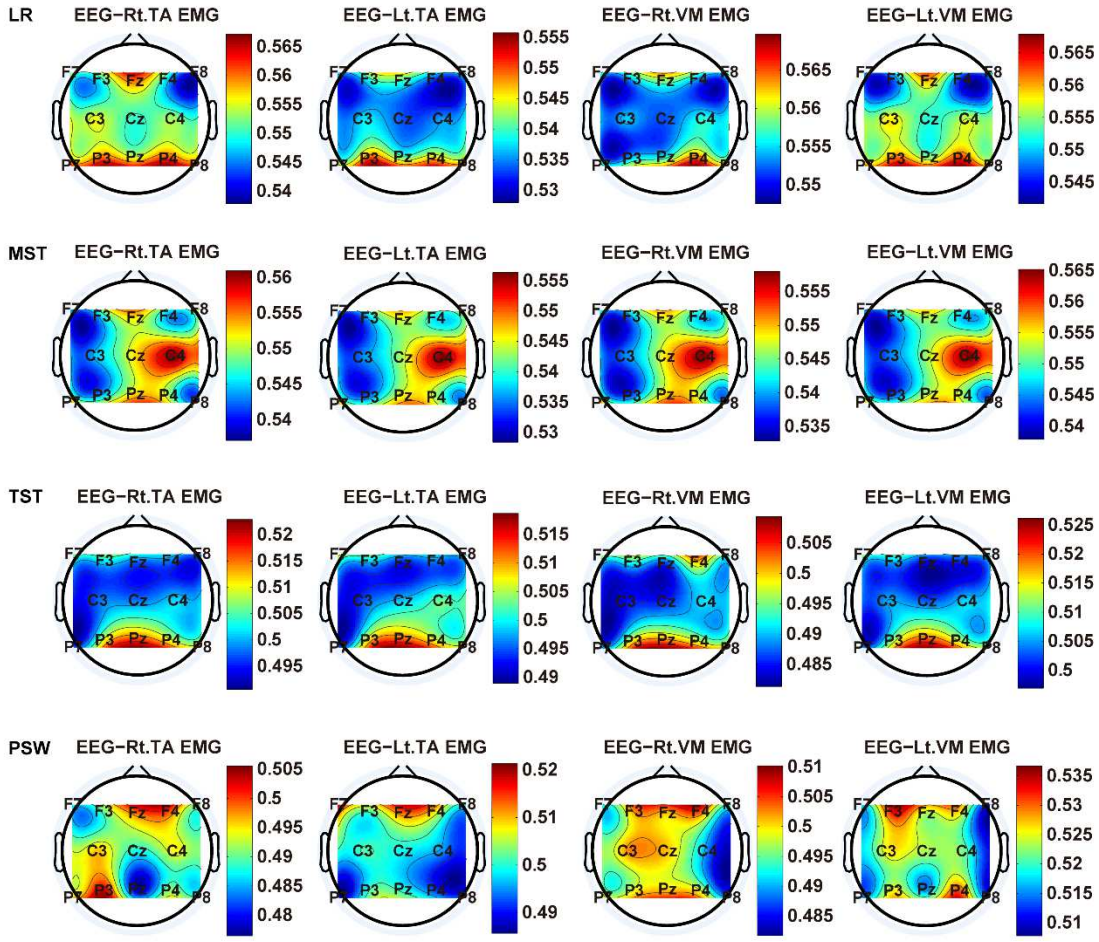

Fig. 8 The TFCMI topography between EEG (beta band) and sEMG (TA, VM) of the stance phase (LR, MST, TST, PSW).

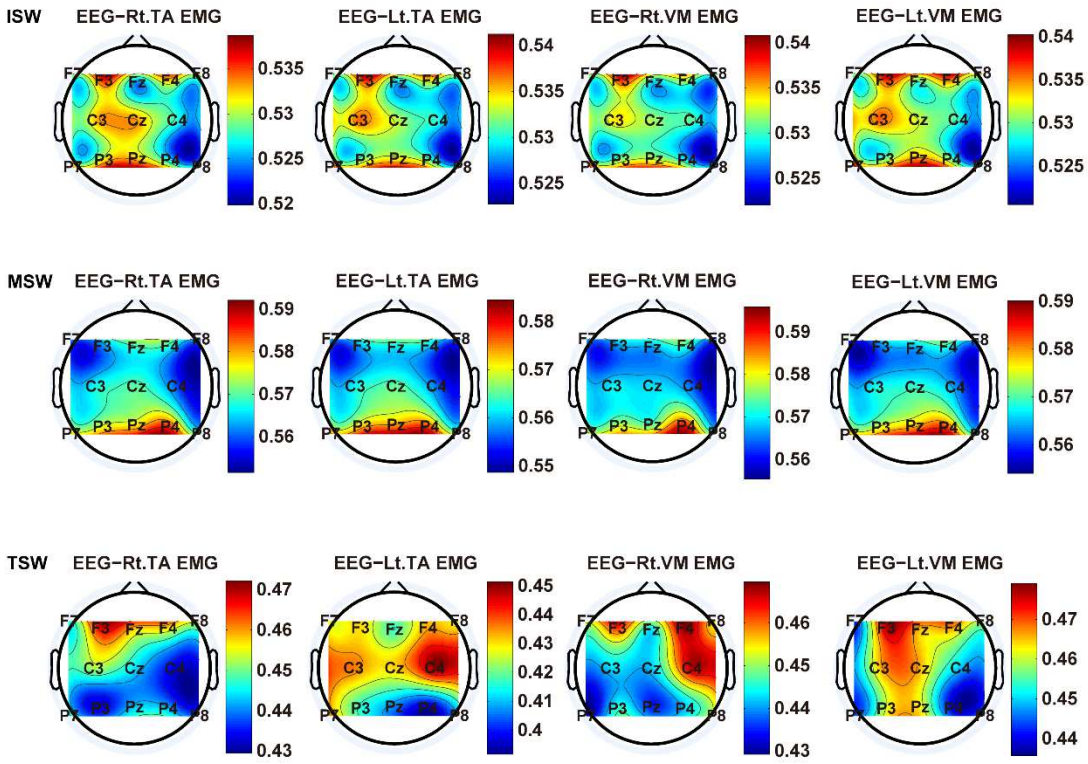

Fig. 9 The TFCMI topography between EEG (beta band) and sEMG (TA, VM) of the swing phase (ISW, MSW, TSW).

In Figures 10 and 11, we can observe that the distribution of TFCMI values between EEG and BF differs from that between EEG and GM in PSW and TSW. Table 2 shows the sEMG channels most related to the EEG channels in PSW and TSW.

Table 2 sEMG channels most related to EEG channels in PSW and TSW

Gait phases	sEMG channels	Most related EEG channels
PSW	Rt.BF	P3, P7
	Lt.BF	F4

	Rt.GM	P3, Pz
	Lt.GM	F3, Fz, Cz, P3, P4, Pz
TSW	Rt.BF	F8
	Lt.BF	F3, Fz, F4, P3
	Rt.GM	F4, F8, Cz, P3
	Lt.GM	Cz

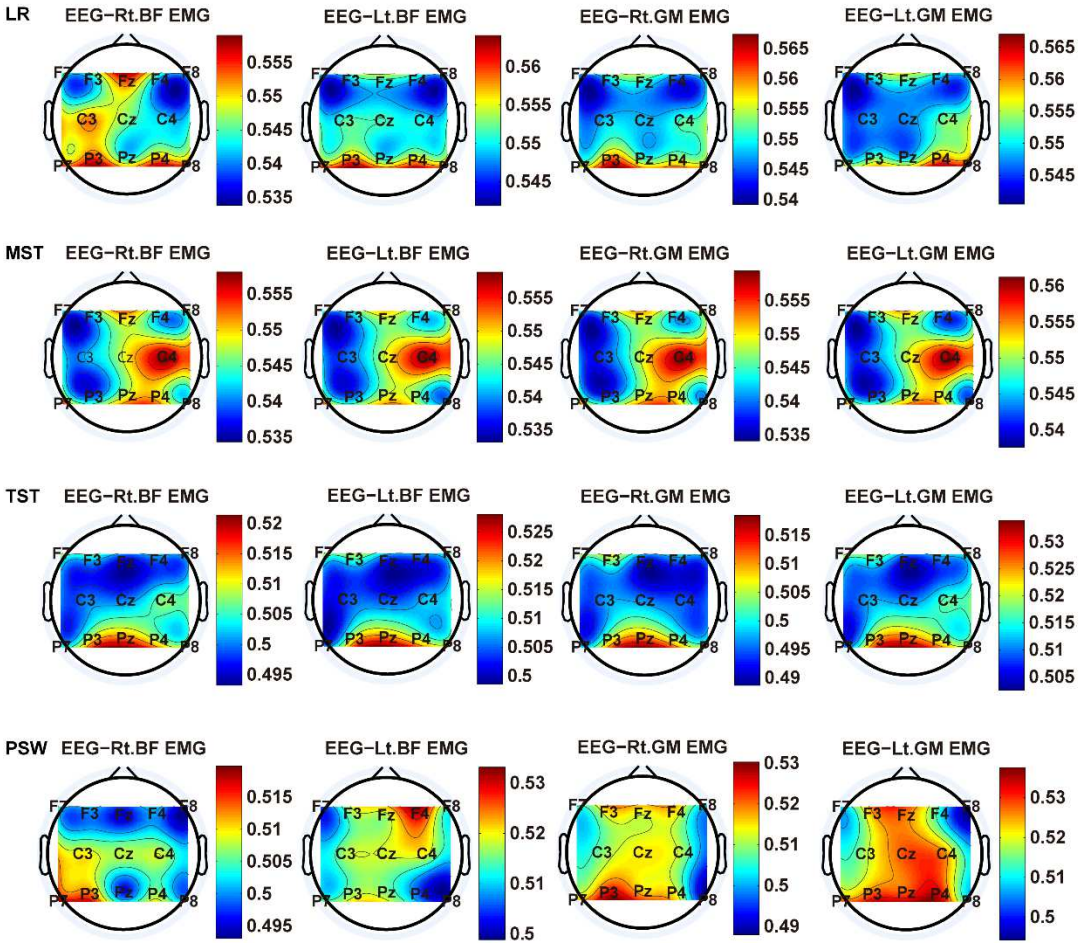

Fig. 10 TFCMI topography between EEG (beta band) and sEMG (BF, GM) of the stance phase (LR, MST, TST, PSW).

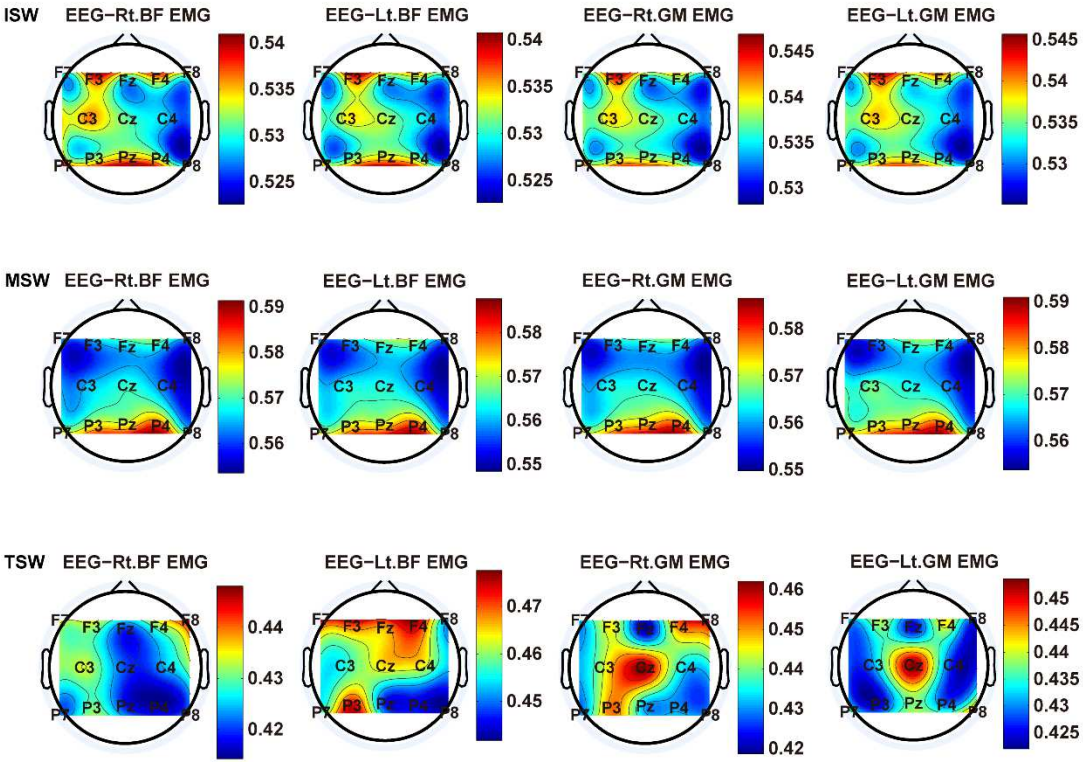

Fig. 11 TFCMI topography between EEG (beta band) and sEMG (BF, GM) of the stance phase (ISW, MSW, TSW).

TFCMI values of the frontal, central and parietal lobes were calculated and can be seen in Figures 12 (beta band EEG signals) and 13 (gamma band EEG signals). One-Way ANOVA was utilized to explore whether the difference between TFCMI values for the seven gait phases was significant. Figure 12 displays the results of the One-Way ANOVA, where we can see that the difference between TFCMI values for the seven gait phases was significant: Lt.TA: F=405.155, p <0.05; Lt.VM: F=375.047, p <0.05; Lt.BF: F=325.468, p <0.05; Lt.GM: F=458.239, p <0.05; Rt.TA: F=503.750, p <0.05; Rt.VM: F=522.972, p <0.05; Rt.BF: F=671.044, p <0.05; Rt.GM:

398 F=401.992, p <0.05).

399 Use of post hoc analysis showed that TFCMI value differences between
400 LR and MST, TST and PSW were not significant (p =0.668, p =0.802) for
401 Lt.TA. TFCMI value differences between LR and MST were also not
402 significant (p =0.075) for Lt.VM. TFCMI value differences between TST
403 and PSW were not significant (p =0.126) for Lt.BF, nor were they
404 significant between LR and MST, TST and PSW (p =0.214, p =0.172) for
405 Lt.GM. TFCMI value differences between TST and PSW were not
406 significant (p =0.135) for Rt.VM, nor for LR and MST, TST and PSW (p
407 =0.475, p =0.763) in Rt.BF. TFCMI value differences between LR and
408 MST were not significant (p =0.095) for Rt.VM. However, the remaining
409 TFCMI values differed significantly from other gait phases (p <0.05) in all
410 sEMG channels.

411 Figure 13 demonstrates that the One-Way ANOVA results for the gamma
412 band were the same as in the beta band.

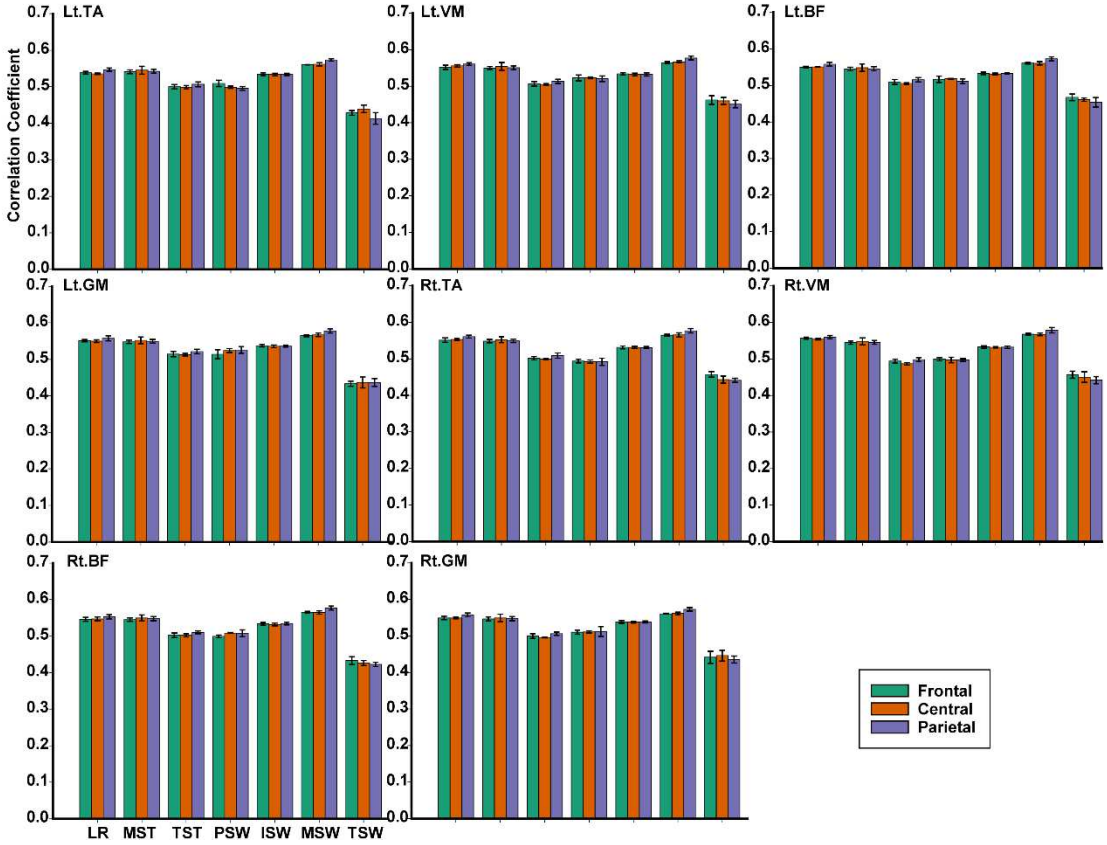

413

414 Fig. 12 TFCMI values (beta band) of the frontal, central and parietal lobes

415 in the seven gait phases for the eight muscles.

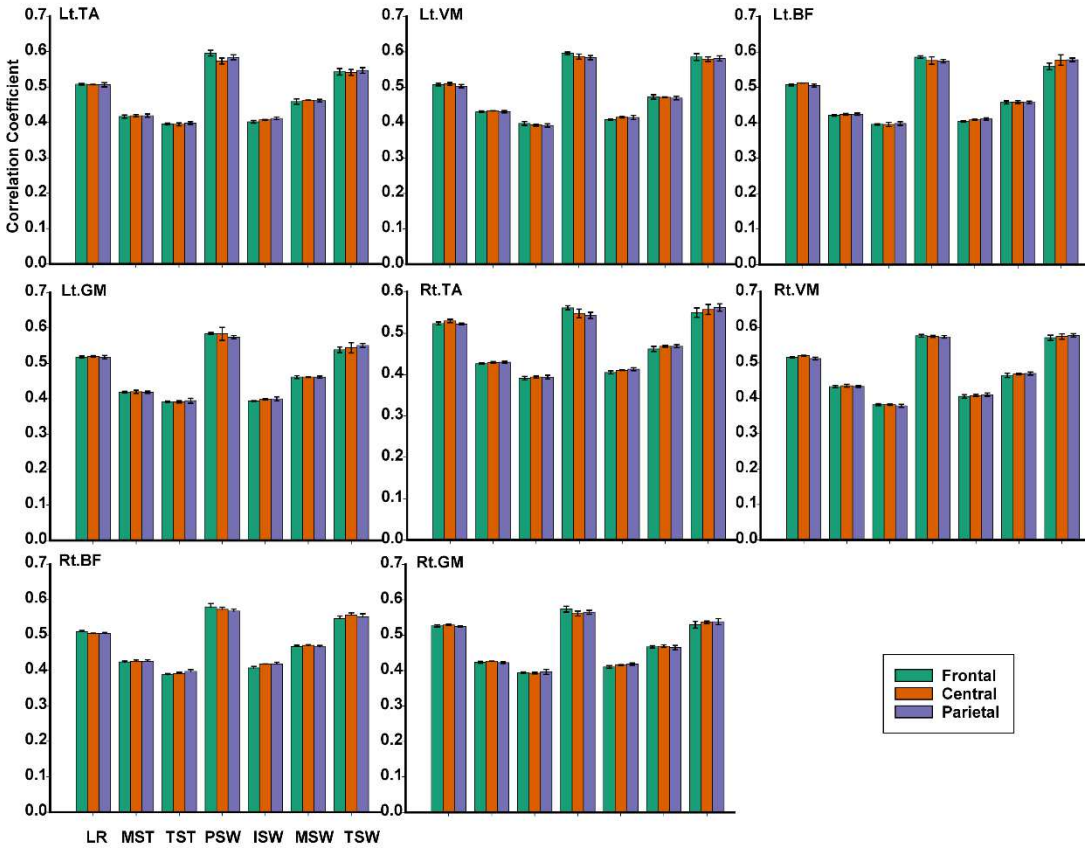

Fig. 13 TFCMI values (gamma band) of the frontal, central and parietal lobes in the seven gait phases for the eight muscles.

Discussion

Gait phase recognition based on the feature set comprising SSC and MPF features of sEMG and SSC feature of EEG were better than recognition based on the feature set comprising SSC and MPF features of sEMG, as shown in Figure 6. Use of near-infrared spectroscopy (NIRS)[43] and functional magnetic resonance imaging (fMRI)[44] have shown that cortex is involved in human walking. This suggests that the addition of SSC features of EEG will enrich gait information contained in sEMG features

and improve the accuracy of gait phase recognition. However, the difference in gait phase recognition between the two feature sets was significant (p=0.017) only at the lowest speed (1.4 km/h). This may be because faster walking speeds reduced alpha and beta band power[45]. Therefore, the contribution of the EEG features to gait phase recognition was reduced at faster rather than slower speeds.

Gait phase recognition for seven participants using SSC and MPF features of sEMG signals as well as SSC feature of EEG signals can be seen in the supplementary material, Figures S1, S2 and S3. Gait phase recognition based on the feature set comprising SSC and MPF features of sEMG were better than that based on the feature set comprising SSC and MPF features of sEMG and SSC feature of EEG in certain gait phases. For instance, gait phase recognition based on the feature without EEG was better than that with EEG in LR for Subject 1 at 2.0 km/h. This suggests a small difference in individuals' level of cortex participation during walking. The feature set comprising SSC and MPF features of sEMG and MPF feature of EEG performed poorly, although the set comprising SSC and MPF features of sEMG as well as SSC features of EEG achieved accurate gait recognition (Fig. 7). This demonstrates that gait phase information weakened when combining sEMG features with MPF of EEG. Therefore, the MPF of EEG is not suitable for fusing with sEMG features to identify gait phase.

Cortical activation is locked to gait cycle, as has been demonstrated by

several researchers[46][47][4]. However, leg muscles control leg movement directly, while cortico-muscular interaction analysis in a fine gait phase was not investigated in the time-frequency domain. The latter is critical for the rehabilitation of gait disorders, especially nontraumatic gait disorders. By computing TFCMI values between EEG and sEMG using beta band EEG data, we found that cortico-muscular connectivity differed between the 13 EEG and the eight sEMG channels at the PSW and TSW gait phases (Figs. 8, 9, 10, 11). Additionally, similar cortex areas were activated in the eight muscles at other gait phases. Previous authors have suggested that cortico-muscular connectivity was stronger in the muscles of swing legs than those of stance legs[4]. Other authors have found that we carry out complex control for keeping our bodies in an upright, dynamic posture during the stance phase[48][49]. These findings do not contradict ours, since in the PSW and TSW gait phases, the end of stance phase and the swing phase respectively, the broader cerebral cortex area is more involved in the regulation of gait than in other gait phases. Muscle-related cortex was identical at other gait phases.

In contrast, the premotor area (PMA) and supplementary motor area (SMA) plan the movement sequence, while the next gait phase is planned by the PMA and SMA at the end of both stance and swing phases[50]. TFCMI topography for gamma band is shown in the supplementary material, Figures S4, S5, S6 and S7. Using gamma band EEG data, we found that

the activated cerebral cortex area crossed with the eight muscles were not the same at each gait phase. This is consistent with previous results. For example, it has been shown that using gamma band features to decode attention during gait is feasible[51].

Cortico-muscular interaction analysis for the seven gait phases has not been previously investigated in the time-frequency domain using TFCMI method. However, it could be asked whether our research is instructive for gait rehabilitation? Additionally, are the differences in TFCMI values significant in the seven gait phases? We calculated TFCMI values for the frontal, central and parietal lobes, results of which can be seen in Figures 12 (beta band EEG signals) and 13 (gamma band EEG signals). We found that TFCMI value differences among the seven gait phases were significant. Our results can guide rehabilitation physicians as they develop a rehabilitation plan for each phase of a patients' gait.

Conclusion

It is necessary to research cortico-muscular interaction in the seven gait phases. We achieved two goals towards addressing this problem: (1) the feature set comprising SSC and MPF features of sEMG and SSC feature of EEG is recommended for identifying the seven gait phases for seven individuals; (2) use of TFCMI analysis proved that BF, VM, TA and GM correlated to different cortices in PSW and TSW, which is a novel finding.

TFCMI values for frontal, central and parietal lobes were calculated and displayed in Figures 12 and 13. We found that the difference between TFCMI values among the seven gait phases was significant. The finding of this study proved that a ‘fine’ gait phase control during treadmill walking by motor cortex is available. This can be applied to a gait rehabilitation device for people with gait disorders.

Declarations

Ethics approval and consent to participate

All study procedures performed were approved by the Institutional Review Boards of Xi’an Jiaotong University and carried out according to the Helsinki Declaration of 1975. All participants approved the study procedures.

Consent for publication

All authors consent for publication.

Availability of data and material

The research data is not available due to further analysis of the data is needed for us.

Competing interests

Declarations of interest: none.

Funding

This work was supported by the Equipment Advance Research Foundation of China [grant numbers 61400030701] and the Fundamental Research Funds for the Central Universities [grant numbers sxzy022019050].

Author Contributions

PW designed the study, conducted and supervised the experimental process, analyzed the experimental data and wrote this paper. JZ guided the experimental process. BW co-designed the study. JH supervised data analysis. All authors revised and approved the manuscript.

Acknowledgments

The authors thank the participants who enrolled in these experiments.

References

[1] D. R. Louie and J. J. Eng, “Powered robotic exoskeletons in post-stroke rehabilitation of gait: A scoping review,” *J. Neuroeng. Rehabil.*, vol. 13, no. 1, pp. 1–10, 2016.

[2] J. Ziegler, H. Gattringer, and A. Mueller, “Classification of Gait

528 Phases Based on Bilateral EMG Data Using Support Vector
529 Machines," pp. 978–983, 2018.
530 [3] I. H. Chen, Y. R. Yang, C. F. Lu, and R. Y. Wang, "Novel gait
531 training alters functional brain connectivity during walking in
532 chronic stroke patients: A randomized controlled pilot trial 11
533 Medical and Health Sciences 1109 Neurosciences 11 Medical and
534 Health Sciences 1103 Clinical Sciences," *J. Neuroeng. Rehabil.*,
535 vol. 16, no. 1, pp. 1–14, 2019.
536 [4] F. Artoni *et al.*, "Unidirectional brain to muscle connectivity reveals
537 motor cortex control of leg muscles during stereotyped walking,"
538 *Neuroimage*, vol. 159, no. August, pp. 403–416, 2017.
539 [5] J. C. Bradford, J. R. Lukos, and D. P. Ferris, "Electrocortical
540 activity distinguishes between uphill and level walking in humans,"
541 *J. Neurophysiol.*, vol. 115, no. 2, pp. 958–966, 2016.
542 [6] J. T. Gwin, K. Gramann, S. Makeig, and D. P. Ferris,
543 "Electrocortical activity is coupled to gait cycle phase during
544 treadmill walking," *Neuroimage*, vol. 54, no. 2, pp. 1289–1296,
545 2011.
546 [7] C. la Fougère *et al.*, "Real versus imagined locomotion: A [18F]-
547 FDG PET-fMRI comparison," *Neuroimage*, vol. 50, no. 4, pp.
548 1589–1598, 2010.
549 [8] S. Stuart, L. Alcock, L. Rochester, R. Vitorio, and A. Pantall,

"Monitoring multiple cortical regions during walking in young and older adults: Dual-task response and comparison challenges," *Int. J. Psychophysiol.*, vol. 135, no. April 2018, pp. 63–72, 2019.

[9] H. Reimann, T. Fettrow, E. D. Thompson, and J. J. Jeka, "Neural control of balance during walking," *Front. Physiol.*, vol. 9, no. SEP, pp. 1–13, 2018.

[10] B. Brouwer, K. Parvataneni, and S. J. Olney, "A comparison of gait biomechanics and metabolic requirements of overground and treadmill walking in people with stroke," *Clin. Biomech.*, vol. 24, no. 9, pp. 729–734, Nov. 2009.

[11] P. Jensen, N. J. Jensen, C. U. Terkildsen, J. T. Choi, J. B. Nielsen, and S. S. Geertsen, "Increased central common drive to ankle plantar flexor and dorsiflexor muscles during visually guided gait," *Physiol. Rep.*, vol. 6, no. 3, pp. 1–11, 2018.

[12] P. Jensen *et al.*, "Using Corticomuscular and Intermuscular Coherence to Assess Cortical Contribution to Ankle Plantar Flexor Activity During Gait," *J. Mot. Behav.*, vol. 0, no. 0, pp. 1–13, 2019.

[13] J. Wagner, T. Solis-Escalante, P. Grieshofer, C. Neuper, G. Müller-Putz, and R. Scherer, "Level of participation in robotic-assisted treadmill walking modulates midline sensorimotor EEG rhythms in able-bodied subjects," *Neuroimage*, vol. 63, no. 3, pp. 1203–1211, 2012.

[14] J. Wagner, T. Solis-Escalante, R. Scherer, C. Neuper, and G. Müller-Putz, “It’s how you get there: Walking down a virtual alley activates premotor and parietal areas,” *Front. Hum. Neurosci.*, vol. 8, no. 1 FEB, pp. 1–11, 2014.

[15] S. Stuart, R. Vitorio, R. Morris, D. N. Martini, P. C. Fino, and M. Mancini, “Cortical activity during walking and balance tasks in older adults and in people with Parkinson’s disease: A structured review,” *Maturitas*, vol. 113, no. April, pp. 53–72, 2018.

[16] D. Popivanov and J. Dushanova, “Non-linear EEG dynamic changes and their probable relation to voluntary movement organization,” *Neuroreport*, vol. 10, no. 7, pp. 1397–1401, 1999.

[17] C. C. Chen *et al.*, “Mutual-Information-Based Approach for Neural Connectivity during Self-Paced Finger Lifting Task,” *Hum. Brain Mapp.*, vol. 29, no. 3, pp. 265–280, 2008.

[18] “Time – Frequency Cross Mutual Information Analysis of the Brain,” vol. 50, no. 3, 2018.

[19] C. F. Lu *et al.*, “Reorganization of functional connectivity during the motor task using EEG time-frequency cross mutual information analysis,” *Clin. Neurophysiol.*, vol. 122, no. 8, pp. 1569–1579, 2011.

[20] J. Taborri, E. Palermo, S. Rossi, and P. Cappa, “Gait partitioning methods: A systematic review,” *Sensors (Switzerland)*, vol. 16, no.

1, pp. 40–42, 2016.

[21] P. C. Formento, R. Acevedo, S. Ghoussayni, and D. Ewins, “Gait event detection during stair walking using a rate gyroscope,” *Sensors (Switzerland)*, vol. 14, no. 3, pp. 5470–5485, 2014.

[22] R. W. Selles, M. A. G. Formanoy, J. B. J. Bussmann, P. J. Janssens, and H. J. Stam, “Automated estimation of initial and terminal contact timing using accelerometers; development and validation in transtibial amputees and controls,” *IEEE Trans. Neural Syst. Rehabil. Eng.*, vol. 13, no. 1, pp. 81–88, 2005.

[23] J. M. Jasiewicz *et al.*, “Gait event detection using linear accelerometers or angular velocity transducers in able-bodied and spinal-cord injured individuals,” *Gait Posture*, vol. 24, no. 4, pp. 502–509, 2006.

[24] Y. Li, F. Gao, H. Chen, and M. Xu, “Gait recognition based on EMG with different individuals and sample sizes,” *Chinese Control Conf. CCC*, vol. 2016-Augus, pp. 4068–4072, 2016.

[25] P. na Wei, R. Xie, R. Tang, C. Li, J. Kim, and M. Wu, “sEMG Based Gait Phase Recognition for Children with Spastic Cerebral Palsy,” *Ann. Biomed. Eng.*, 2018.

[26] J. Rouillard *et al.*, “Hybrid BCI Coupling EEG and EMG for Severe Motor Disabilities,” *Procedia Manuf.*, vol. 3, no. Ahfe, pp. 29–36, 2015.

[27] Y. Gao, L. Ren, R. Li, and Y. Zhang, “Electroencephalogram-electromyography coupling analysis in stroke based on symbolic transfer entropy,” *Front. Neurol.*, vol. 8, no. JAN, 2018.

[28] J. Choi and H. Kim, “Real-Time Decoding of EEG Gait Intention for Controlling a Lower-limb Exoskeleton System,” *7th Int. Winter Conf. Brain-Computer Interface, BCI 2019*, pp. 1–3, 2019.

[29] A. E. Study, G. R. Figueiredo, D. Campos, W. L. Ripka, and L. Ulbricht, *Attentional Bias for Faces in Relation*. Springer Singapore, 2019.

[30] A. S. Oliveira, F. G. Arguissain, and O. K. Andersen, “Cognitive Processing for Step Precision Increases Beta and Gamma Band Modulation During Overground Walking,” *Brain Topogr.*, vol. 31, no. 4, pp. 661–671, 2018.

[31] J. Li *et al.*, “What Are Spectral and Spatial Distributions of EEG-EMG Correlations in Overground Walking? An Exploratory Study,” *IEEE Access*, vol. 7, pp. 1–1, 2019.

[32] J. Perry, S. T. k, and J. R. Davids, “Gait Analysis: Normal and Pathological Function,” *J. Pediatr. Orthop.*, vol. 12, no. 6, 1992.

[33] T. H. Petersen, M. Willerslev-Olsen, B. A. Conway, and J. B. Nielsen, “The motor cortex drives the muscles during walking in human subjects,” *J. Physiol.*, vol. 590, no. 10, pp. 2443–2452, 2012.

[34] A. Delorme and S. Makeig, “EEGLAB: An open source toolbox for

638 analysis of single-trial EEG dynamics including independent
639 component analysis," *J. Neurosci. Methods*, vol. 134, no. 1, pp. 9–
640 21, 2004.
641 [35] J. E. Kline, H. J. Huang, K. L. Snyder, and D. P. Ferris, "Isolating
642 gait-related movement artifacts in electroencephalography during
643 human walking," *J. Neural Eng.*, vol. 12, no. 4, p. 46022, 2015.
644 [36] L. Sun, Y. Liu, and P. J. Beadle, "Independent component analysis
645 of EEG signals," *Proc. 2005 IEEE Int. Work. VLSI Des. Video*
646 *Technol. IWVDVT 2005*, pp. 293–296, 2005.
647 [37] M. Asghari Oskoei and H. Hu, "Myoelectric control systems-A
648 survey," *Biomed. Signal Process. Control*, vol. 2, no. 4, pp. 275–
649 294, 2007.
650 [38] A. Phinyomark, R. N. Khushaba, E. Ibáñez-Marcelo, A. Patania, E.
651 Scheme, and G. Petri, "Navigating features: A topologically
652 informed chart of electromyographic features space," *J. R. Soc.*
653 *Interface*, vol. 14, no. 137, 2017.
654 [39] R. Martín-Clemente, J. Olias, D. B. Thiyam, A. Cichocki, and S.
655 Cruces, "Information theoretic approaches for motor-imagery BCI
656 systems: Review and experimental comparison," *Entropy*, vol. 20,
657 no. 1, 2018.
658 [40] F. B. Vialatte *et al.*, "A machine learning approach to the analysis
659 of time-frequency maps, and its application to neural dynamics,"

Neural Networks, vol. 20, no. 2, pp. 194–209, 2007.

[41] A. M. Fraser, “Andrew M. Fraser and Harry L. Swinney,” *Phys. Rev. A*, vol. 33, no. 2, pp. 1134–1140, 1986.

[42] L. M. Tamburri, C. D. Hix, and M. Lou Sole, “Revising a book chapter written by a previous author.,” *Nurse Author Ed.*, vol. 12, no. 3, pp. 7–9, 2002.

[43] I. Miyai *et al.*, “Cortical mapping of gait in humans: A near-infrared spectroscopic topography study,” *Neuroimage*, vol. 14, no. 5, pp. 1186–1192, 2001.

[44] R. Cunnington, C. Windischberger, and E. Moser, “Premovement activity of the pre-supplementary motor area and the readiness for action: Studies of time-resolved event-related functional MRI,” *Hum. Mov. Sci.*, vol. 24, no. 5–6, pp. 644–656, 2005.

[45] A. D. Nordin, W. D. Hairston, and D. P. Ferris, “Faster gait speeds reduce alpha and beta EEG spectral power from human sensorimotor cortex,” *IEEE Trans. Biomed. Eng.*, pp. 1–1, 2019.

[46] J. T. Gwin, K. Gramann, S. Makeig, and D. P. Ferris, “Electrocortical activity is coupled to gait cycle phase during treadmill walking,” *Neuroimage*, vol. 54, no. 2, pp. 1289–1296, 2011.

[47] J. E. Kline, H. J. Huang, K. L. Snyder, and D. P. Ferris, “Cortical spectral activity and connectivity during active and viewed arm and

leg movement," *Front. Neurosci.*, vol. 10, no. MAR, 2016.

[48] B. L. Day, "Vestibular-evoked postural responses in the absence of somatosensory information," *Brain*, vol. 125, no. 9, pp. 2081–2088, 2002.

[49] C. R. Fetsch, A. H. Turner, G. C. DeAngelis, and D. E. Angelaki, "Dynamic reweighting of visual and vestibular cues during self-motion perception," *J. Neurosci.*, vol. 29, no. 49, pp. 15601–15612, 2009.

[50] W. Tam, T. Wu, Q. Zhao, E. Keefer, and Z. Yang, "Human motor decoding from neural signals: a review," *BMC Biomed. Eng.*, vol. 1, no. 1, pp. 1–22, 2019.

[51] A. Costa-García, E. Iáñez, A. J. del-Ama, A. Gil-Agudo, and J. M. Azorín, "EEG model stability and online decoding of attentional demand during gait using gamma band features," *Neurocomputing*, vol. 360, pp. 151–162, 2019.

Figures

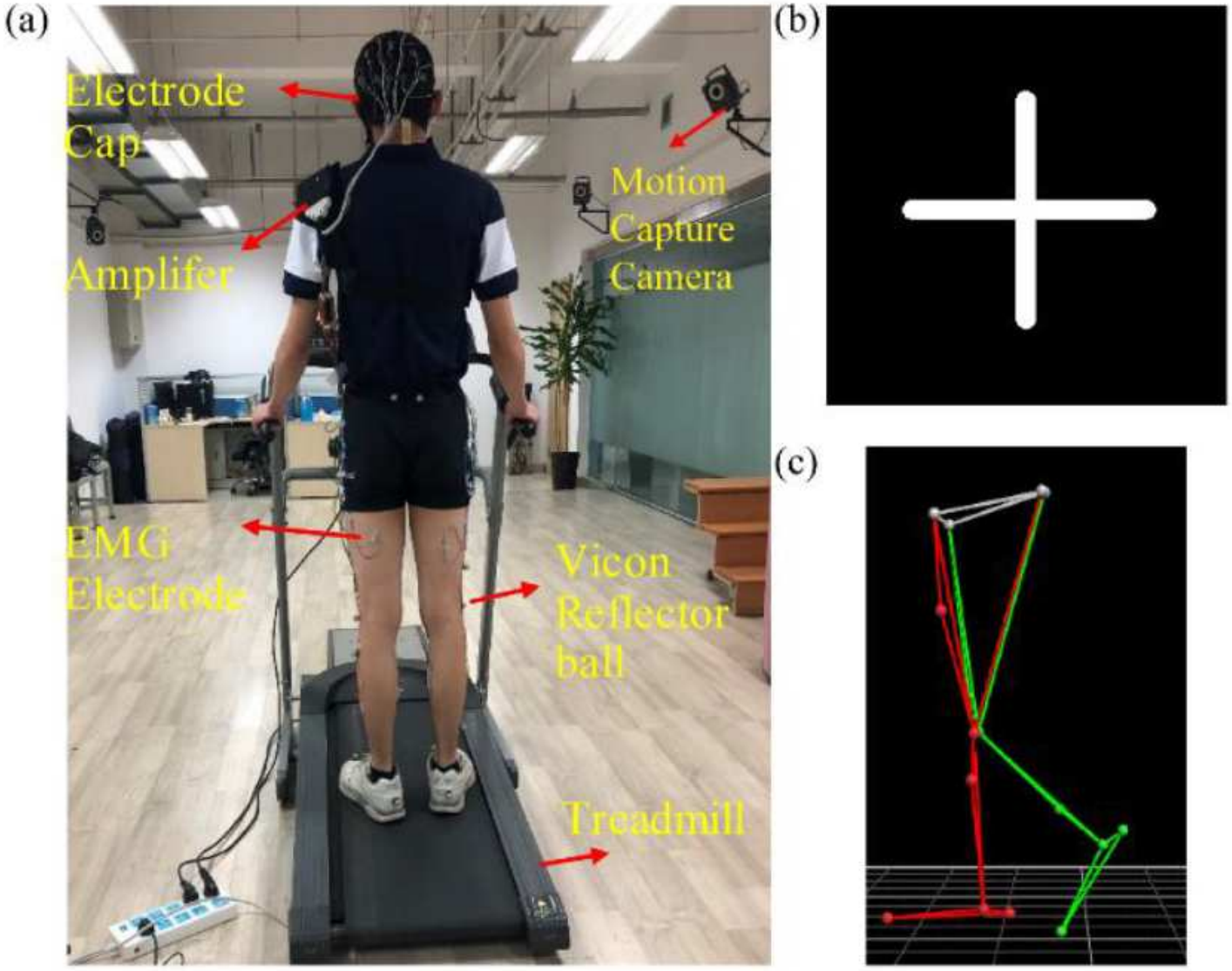

Figure 1

Experimental device, (b) cross symbol, (c) lower limb model in motion capture system .

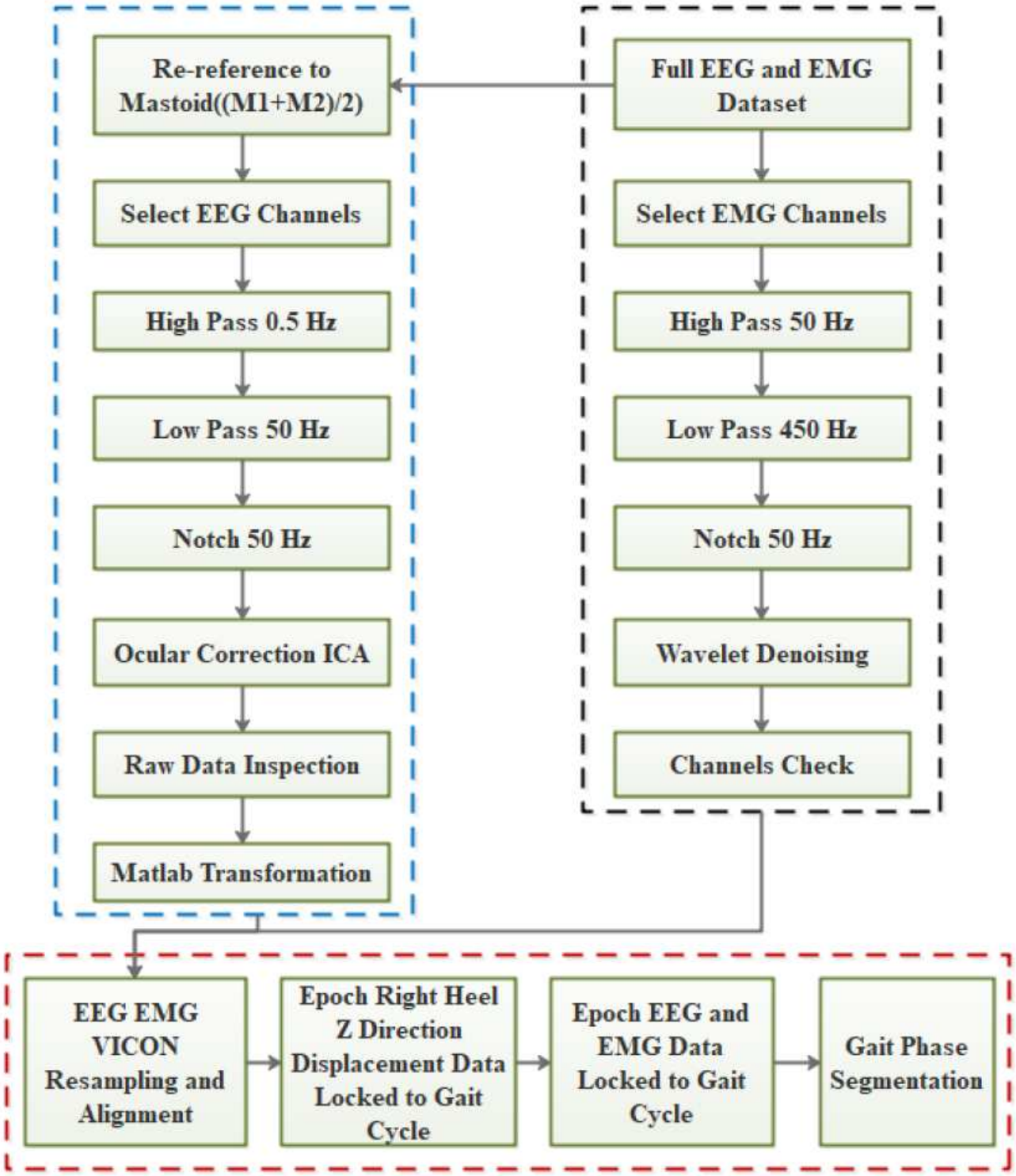

Figure 2

Outline of data processing steps.

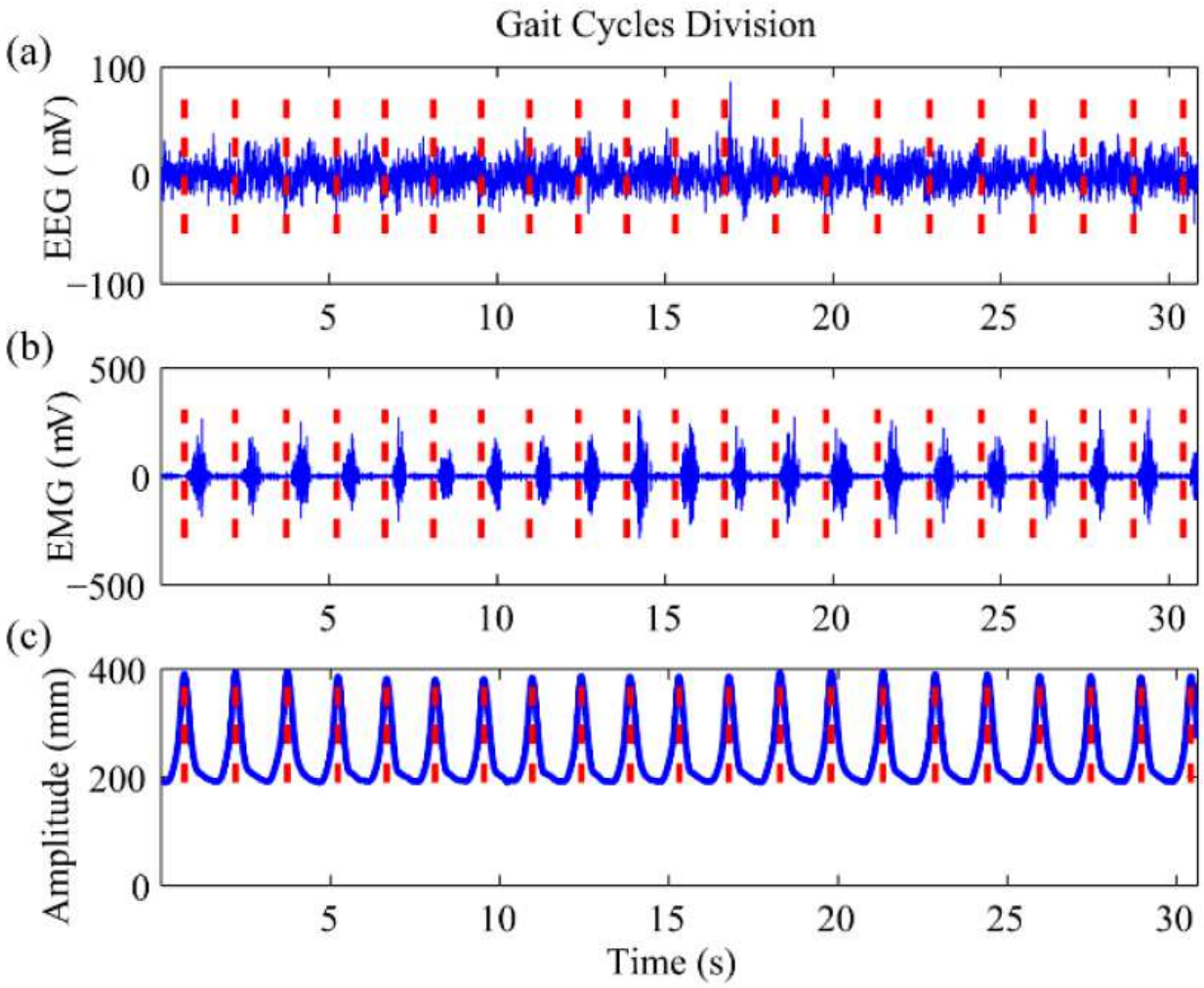

Figure 3

(a) EEG signals, (b) sEMG signals, (c) displacement in z direction of right heel.

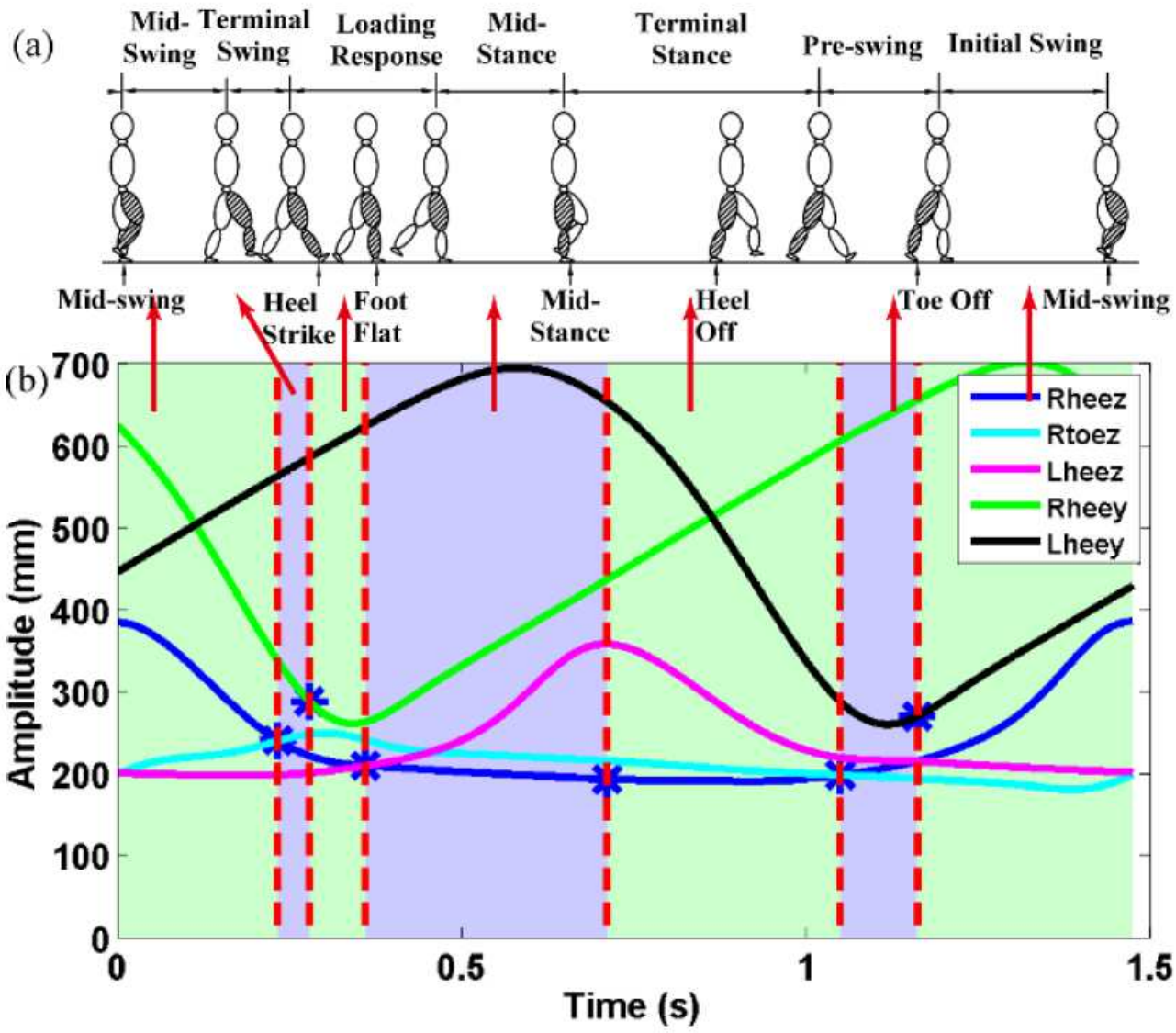

Figure 4

Gait phase division results. (a) S even gait phases of the gait cycle (b) trajectory Feature extraction

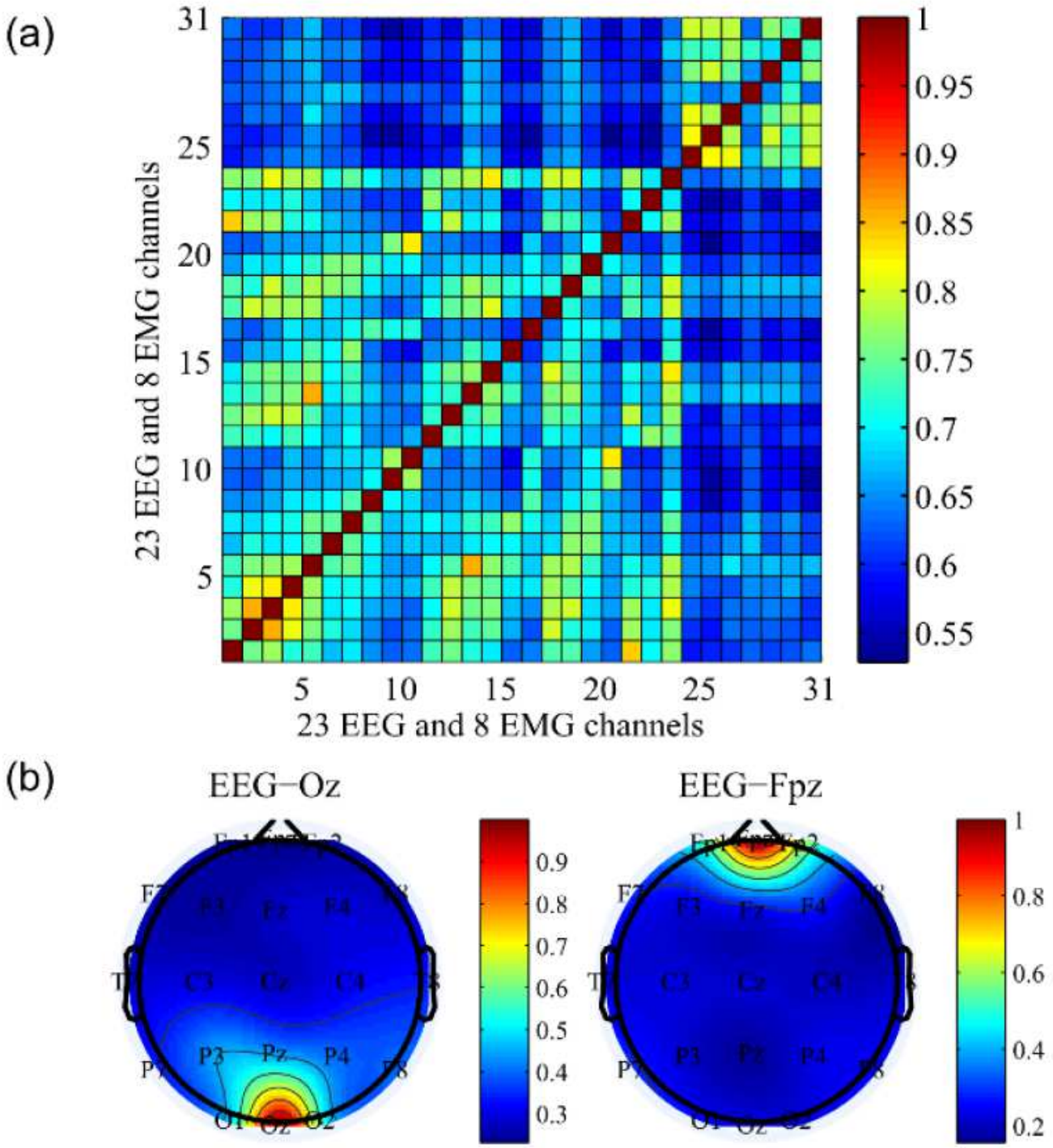

Figure 5

TFCMI computation. (a) TFCMI map, (b) topographic map of mean coupling strength from Oz channel to all EEG channels and Fpz channel to all EEG channels

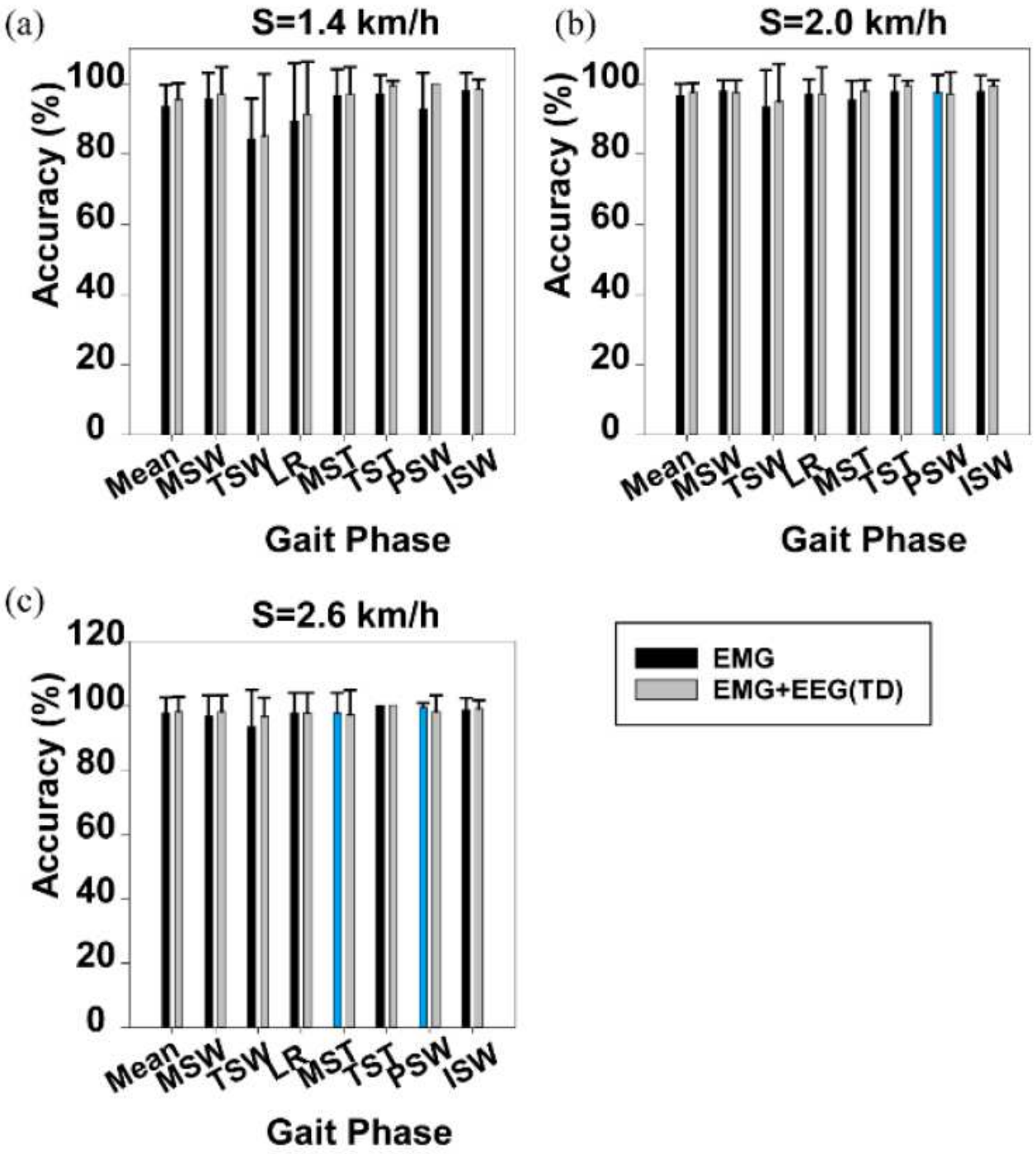

Figure 6

Gait phase recognition results based on the SSC and MPF features of sEMG as well as results based on the SSC and MPF features of sEMG and SSC feature of EEG. (a) Walking speed 1.4 km/h (b) walking speed 2.0 km/h (c) walking speed 2.6 km/h. The blue column indicate s that results based on s EMG features are better than sEMG features combin ed with the EEG feature of SSC.

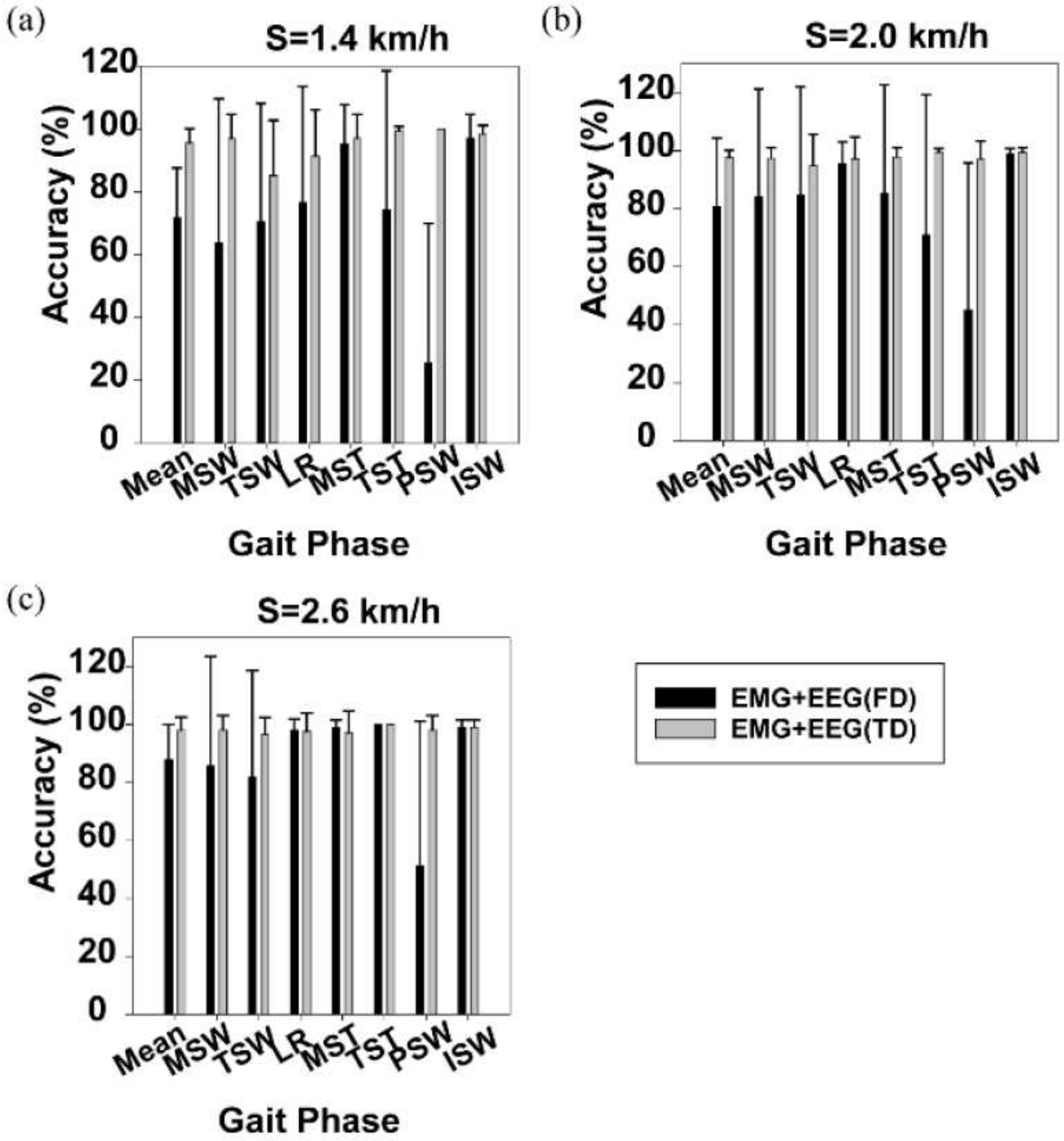

Figure 7

Gait phase recognition based on the SSC and MPF of sEMG and the SSC of EEG as well as gait phase recognition based on the SSC and MPF of sEMG and the MPF of EEG. (a) Walking speed 1.4 km/h (b) walking speed 2.0 km/h (c) walking speed 2.6 km/h

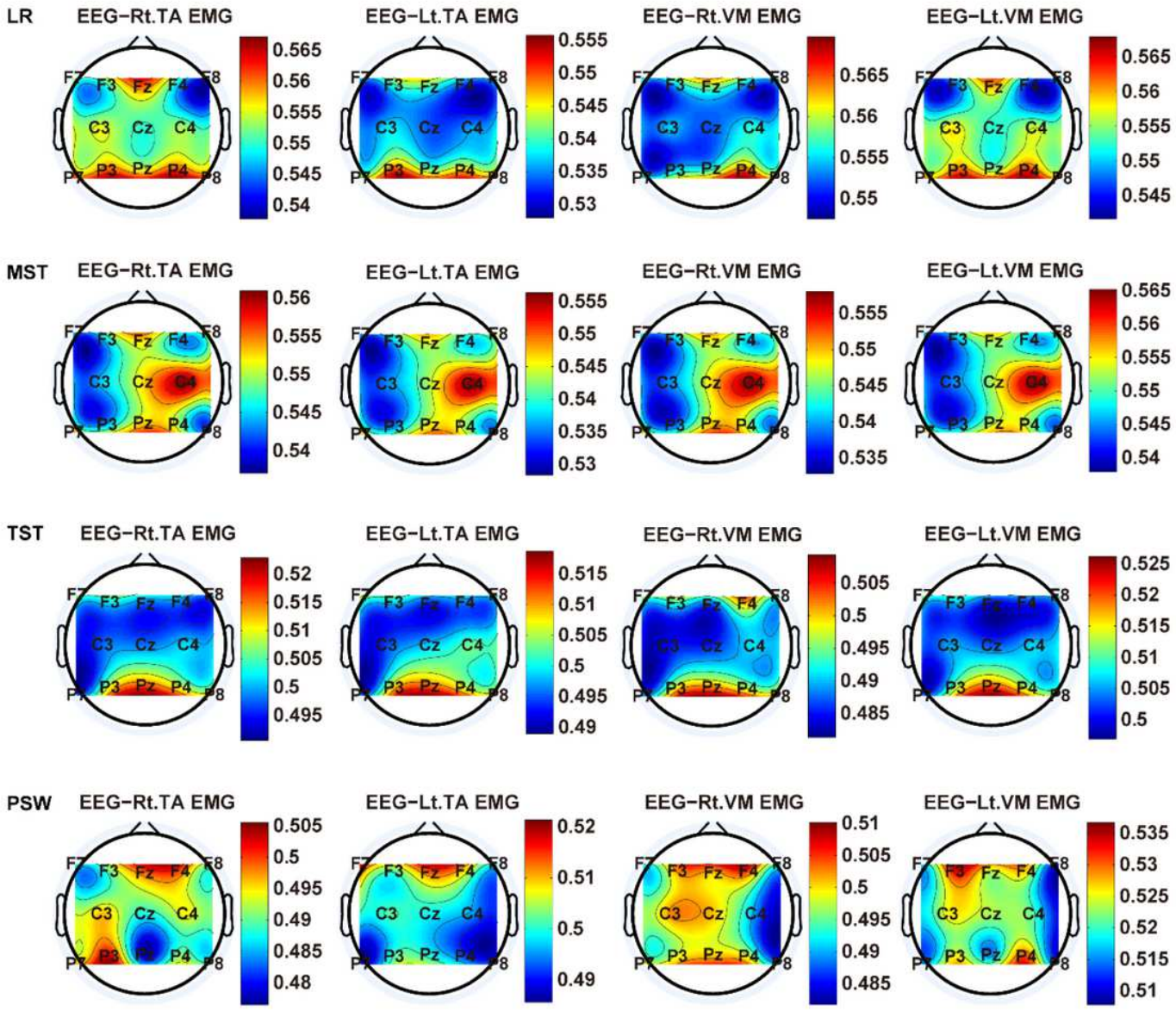

Figure 8

The TFCMI topography between EEG (beta band) and sEMG (TA, VM) of the stance phase (LR, MST, TST, PSW) PSW).

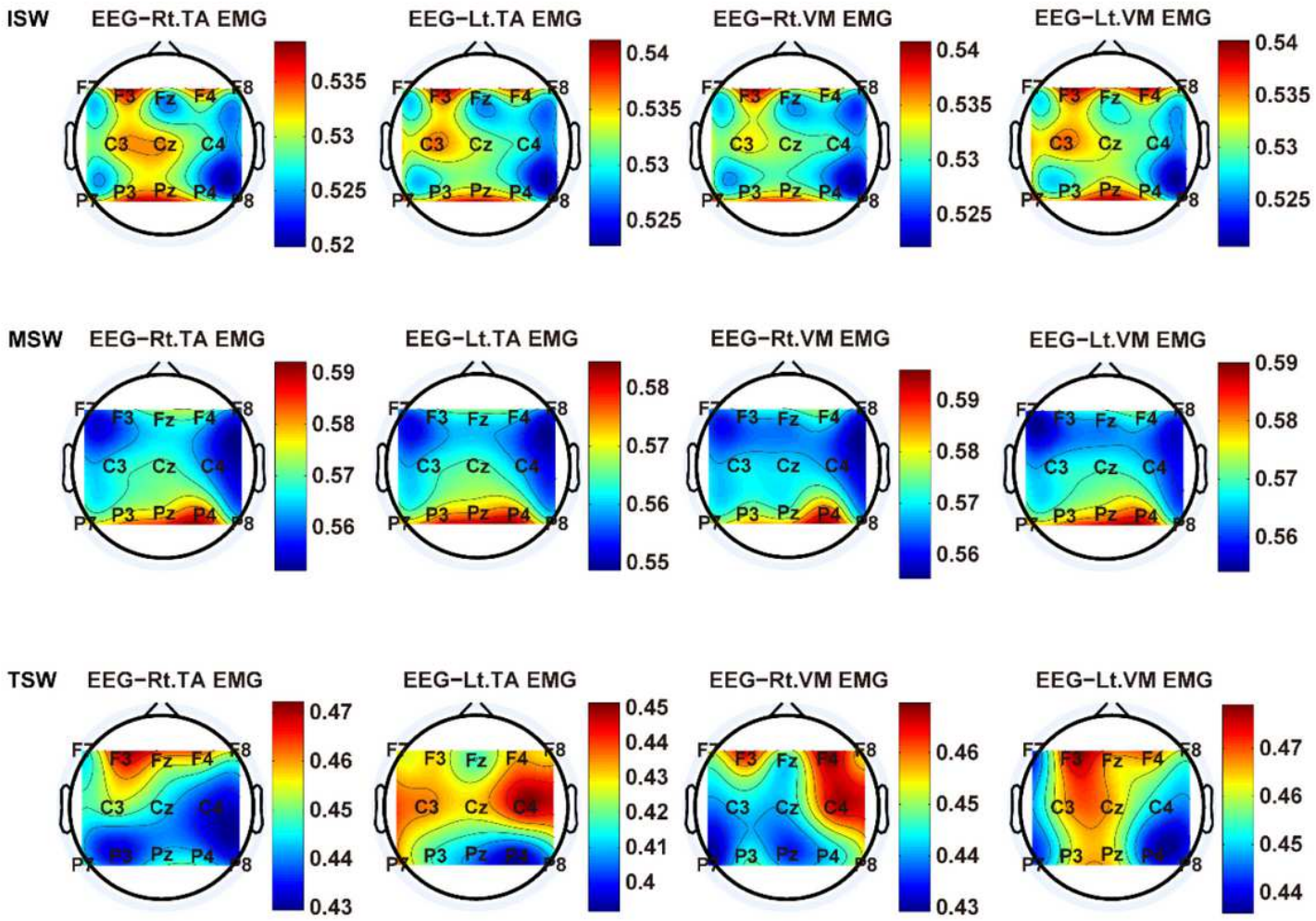

Figure 9

The TFCMI topography between EEG (beta band) and sEMG (TA, VM) of the swing phase (ISW, MSW, TSW) TSW).

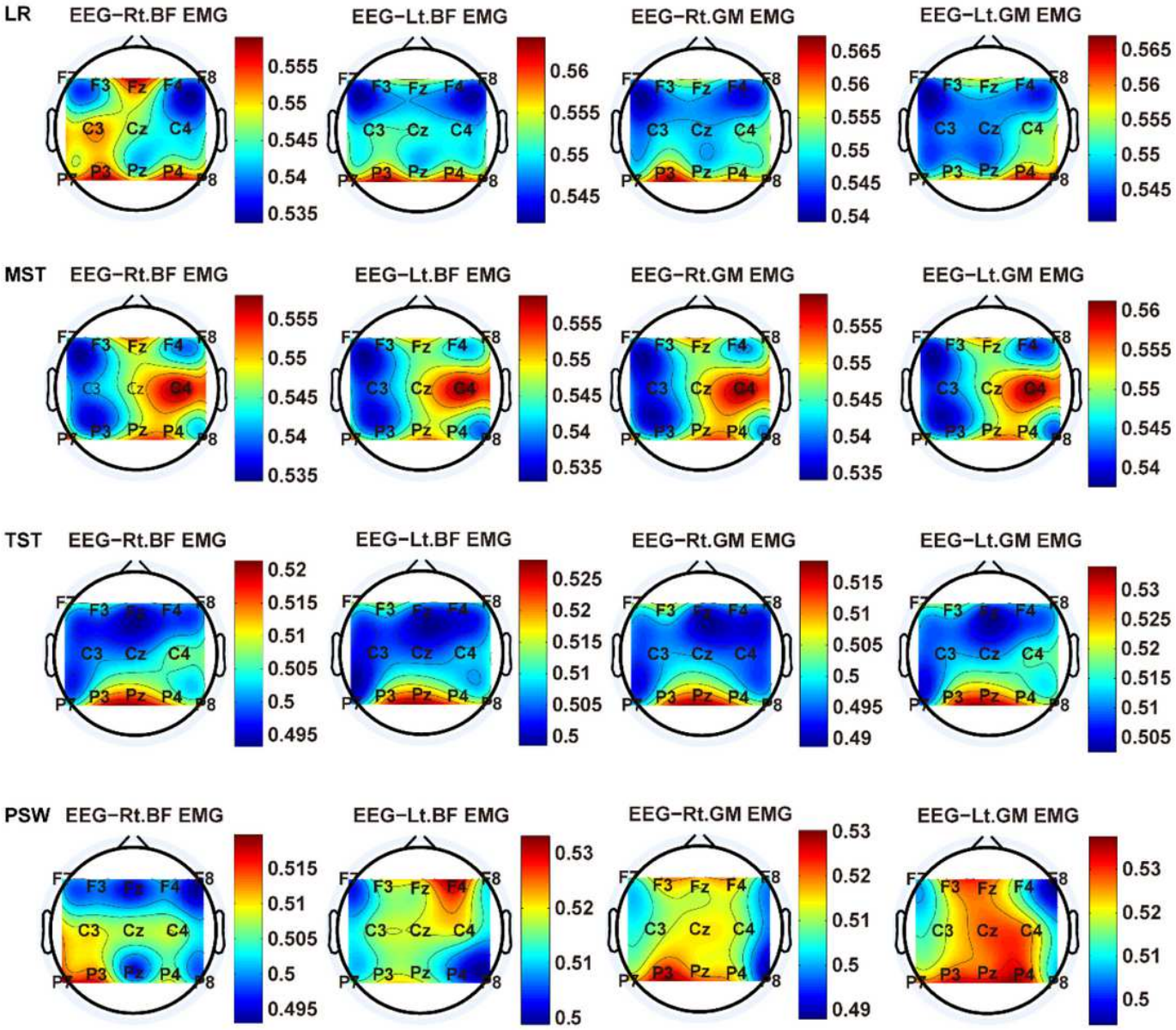

Figure 10

TFCMI topography between EEG (beta band) and sEMG (BF, GM) of the stance phase (LR, MST, TST, PSW) PSW).

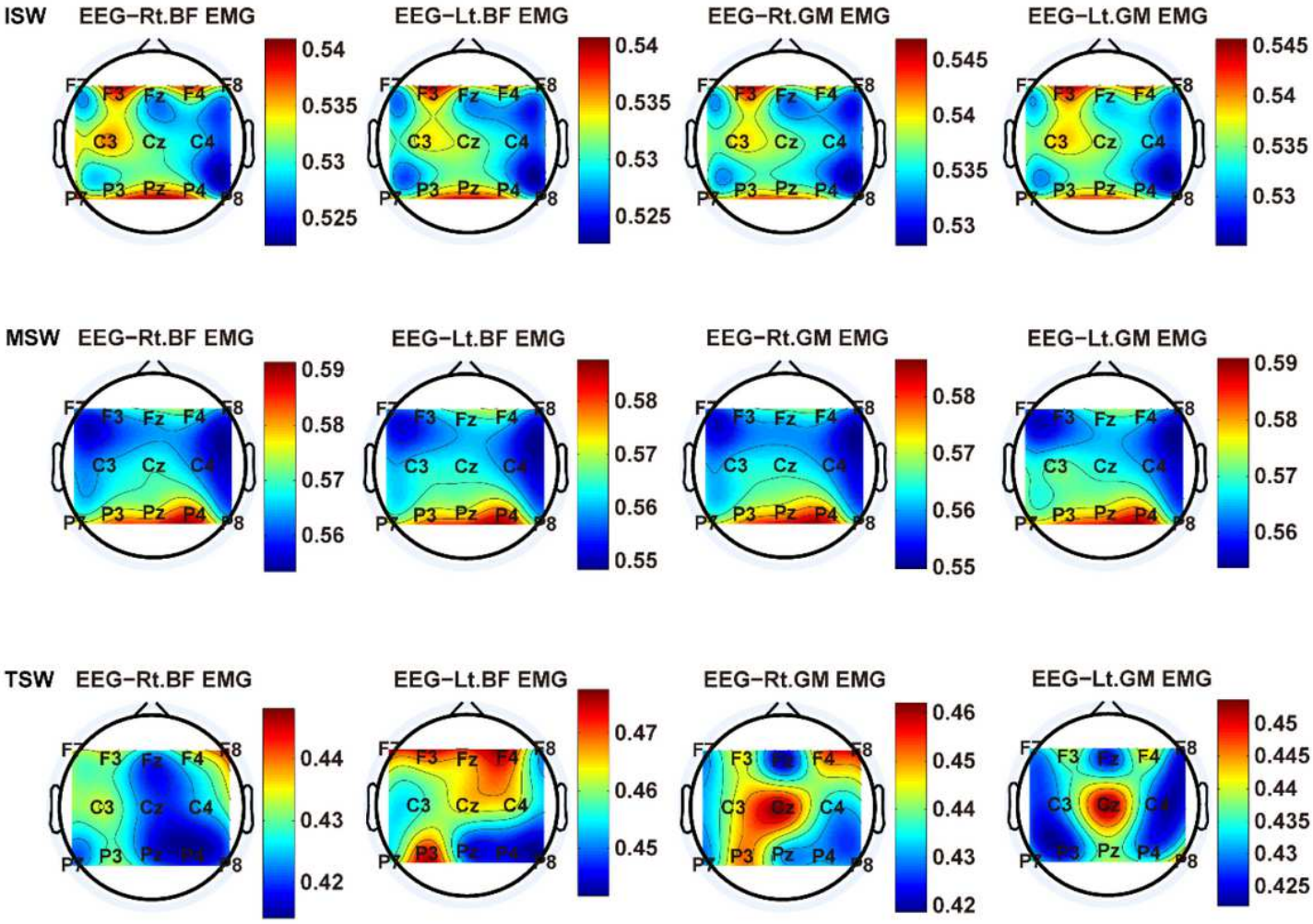

Figure 11

TFCMI topography between EEG (beta band) and sEMG (BF, GM) of the stance phase (ISW, MSW, TSW) TSW).

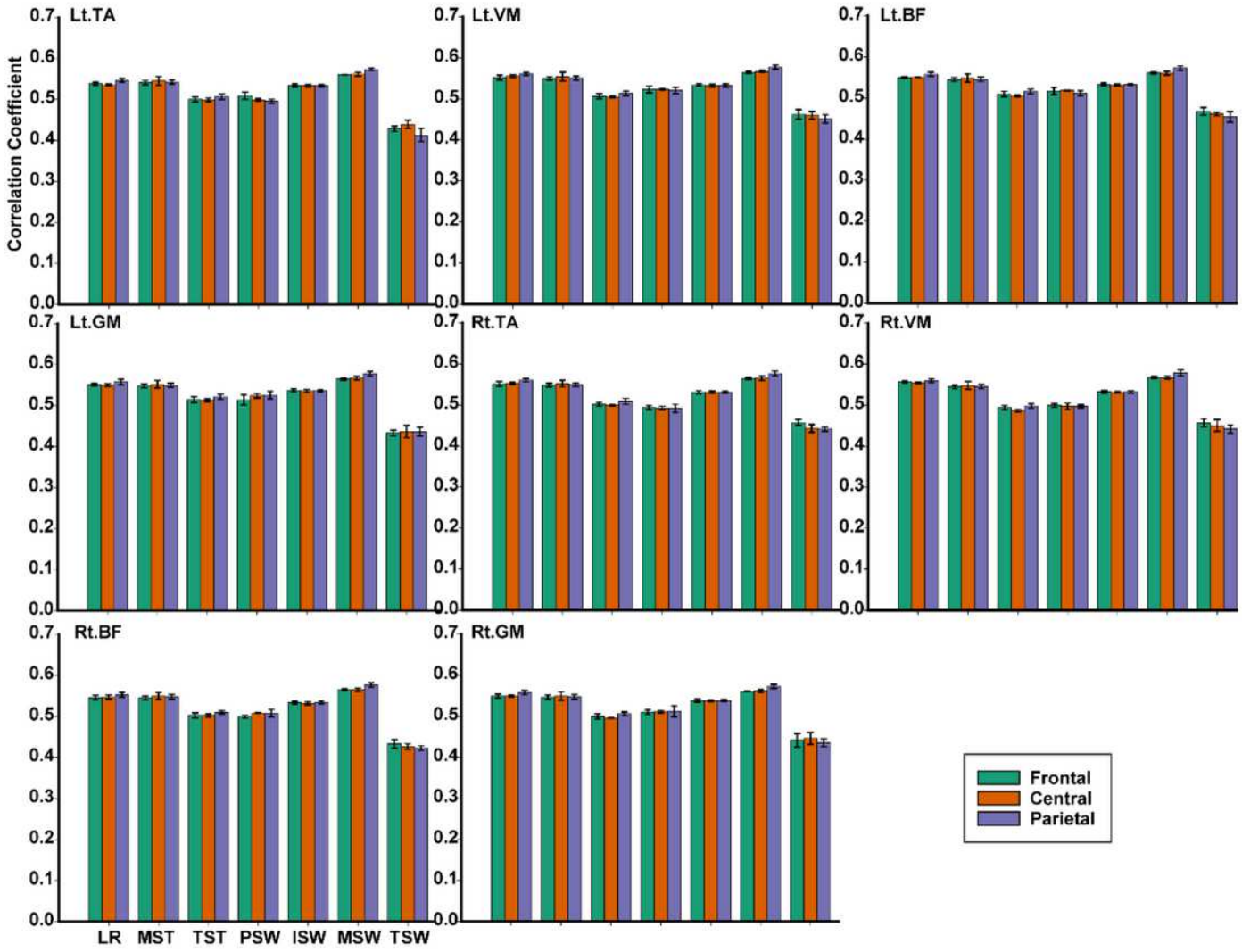

Figure 12

TFCMI values (beta band) of the frontal, central and p arietal lobes in the seven gait phases for the eight muscles.

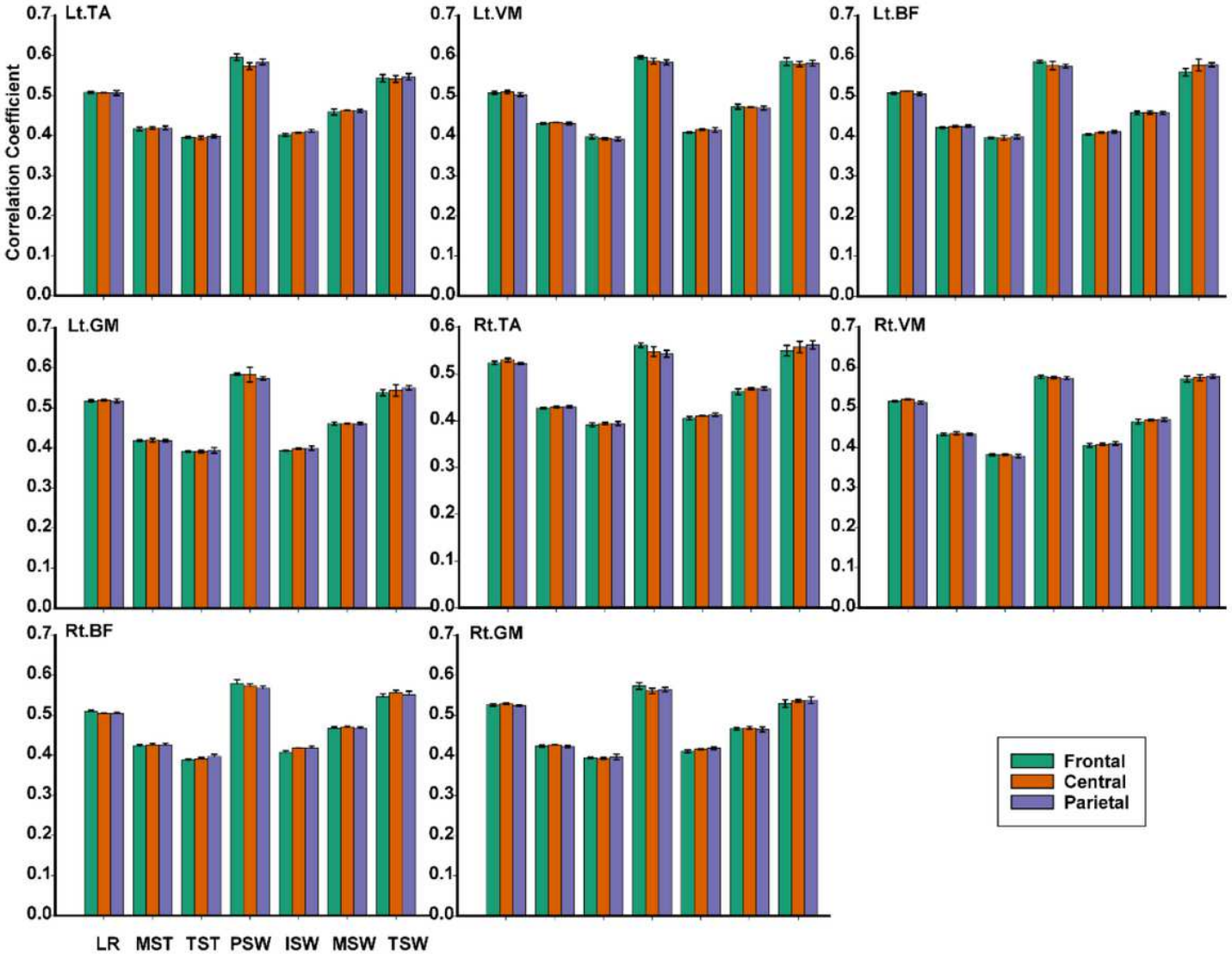

Figure 13

TFCMI values (gamma band) of the frontal, central and p arietal lobes in the seven gait phases for the eight muscles.

Supplementary Files

This is a list of supplementary files associated with this preprint. Click to download.

- FigS4.tif
- FigS3.tif
- FigS7.tif
- FigS1.tif

- FigS2.tif
- FigS5.tif
- FigS6.tif